N-*d* elastic scattering using the hyperspherical harmonics approach with realistic local and nonlocal interactions

L. E. Marcucci,[1,2] A. Kievsky,[2] L. Girlanda,[2] S. Rosati,[1,2] and M. Viviani[2]
[1]*Department of Physics "E. Fermi," University of Pisa, Largo B. Pontecorvo 3, I-56127 Pisa, Italy*
[2]*Istituto Nazionale di Fisica Nucleare, Sezione di Pisa, Largo B. Pontecorvo 3, I-56127 Pisa, Italy*
(Received 21 May 2009; published 16 September 2009)

The application of the hyperspherical harmonic approach to the case of the *N*-*d* scattering problem below deuteron breakup threshold is described. The nuclear Hamiltonian includes two- and three-nucleon interactions, in particular the Argonne v_{18}, the N3LO-Idaho, and the $V_{\text{low}-k}$ two-nucleon, and the Urbana IX and N2LO three-nucleon interactions. Some of these models are local, whereas some are nonlocal. Also electromagnetic effects are included. Accurate calculations for many scattering observables at various center-of-mass energies are performed and the results are compared with the available experimental data. Furthermore, a χ^2 analysis of some of the Hamiltonian models has been performed to compare their capability to describe the scattering process.

DOI: 10.1103/PhysRevC.80.034003 PACS number(s): 21.45.−v, 21.30.−x, 25.10.+s

I. INTRODUCTION

One of the main inputs for any study on nuclear systems within a nonrelativistic framework is the model used to describe the nuclear interaction, i.e., the nuclear Hamiltonian. Nowadays, it is common practice to use, at least for few-nucleon systems, Hamiltonian models composed of a two-nucleon plus, for $A \geqslant 3$, a three-nucleon interaction (TNI). The modern two-nucleon interaction models have a large number of parameters and can reproduce the deuteron properties and the nucleon-nucleon scattering data up to the pion threshold with a χ^2/datum $\simeq$1. Among them, the Argonne v_{18} (AV18) [1] and the charge-dependent Bonn (CDBonn) [2] explicitly include charge-symmetry-breaking terms in the nuclear interaction to reproduce equally well the *np* and *pp* data. Recently, a number of two-nucleon interaction models have been derived by many authors within an effective field theory (EFT) approach, up to next-to-next-to-next-to leading order (N3LO) [3,4]. In particular, the N3LO model of Ref. [4] (N3LO-Idaho) reaches the same level of accuracy of the CDBonn model.

The available models for the TNI contain, on the contrary to the two-nucleon interaction models, a small number of parameters, usually fixed to reproduce the ^{3}H and/or ^{4}He binding energies and, in some cases, the nuclear matter equilibrium density. Among the different existing models, we quote only those ones of the Urbana and Tucson-Melbourne families. Although constructed within different frameworks, these two families of potentials have shown to give similar results, when used in conjunction with a given two-nucleon interaction model. Therefore, we have considered the Urbana IX [5] (UIX) TNI in conjunction with both the AV18 and N3LO-Idaho two-nucleon interaction models. Finally, it should be noted that within the EFT approach mentioned above, TNIs also appear at the next-to-next-to leading order (N2LO) [6]. In particular, we will consider the local version of this N2LO TNI, as given in Ref. [7].

More recently, a new class of two-nucleon interactions has been obtained ($V_{\text{low}-k}$ potentials). With the purpose of eliminating from the semiphenomenological high-precision two-nucleon potentials the high-momentum parts, the two-nucleon Hilbert space has been separated into low- and high-momentum regions and the renormalization group method has been used to integrate out the high-momentum components above a cutoff Λ [8]. The value for Λ is typically fixed in $A > 2$ systems, for example, so that the triton binding energy is reproduced.

At this point, a crucial issue is to test the model for the nuclear Hamiltonian studying $A \geqslant 4$ bound states and $A \geqslant 3$ scattering states. In the present work, we focus our attention to the $A = 3$ scattering problem, which has been the object of a large number of investigations [9]. Traditionally, the $A = 3$ scattering problem with realistic Hamiltonians is solved using the Faddeev equations. However, we have developed in recent years a variational approach, based on the expansion of the wave functions on the hyperspherical harmonics (HH) basis (for a recent review, see Ref. [10]). This method has proven to be very efficient in the description of bound and scattering states in few-nucleon systems. In Ref. [11] the HH expansion with correlations factors (the correlated and pair-correlated HH expansions, CHH and PHH respectively) has been used to describe $A = 3$ bound states, whereas the extension to scattering states has been discussed in Ref. [12]. The inclusion of correlation factors was motivated by the short-range repulsion of the two-nucleon potential that induces particular configurations in the wave function difficult to describe using the bare expansion. In fact, in Ref. [13] the HH expansion without correlation factors has been used to describe the $A = 3$ bound state, with the AV18 interaction. The conclusion was that a much higher number of states are necessary when the bare expansion is used. The same observation has been done in the $A = 4$ system [14] and is a direct consequence of using local interactions, which result to have a strong repulsion at short distances. The implementation of the HH method in momentum-space has been done in Ref. [15] for the $A = 3, 4$ bound states. This analysis has revealed a much faster convergence of the expansion when nonlocal potentials are considered, even when TNI terms are taken into account.

The aim of the present work is twofold. First, we want to extend the HH method to describe N-d scattering states using either local or nonlocal potentials. We will show that we can apply the method in both configuration and momentum spaces. Second, we will present a detailed comparison between the predictions of the different models, local and nonlocal, at low center-of-mass energies, for n-d as well as p-d scattering. Moreover, we will consider the Coulomb potential plus the magnetic moment (MM) interaction that was shown to give sizable contributions [16]. To our knowledge, this is the first time that nonlocal two- plus three-nucleon potentials are used to describe p-d scattering at very low energies.

The article is organized as follows: in Sec. II, the HH method for the low-energy scattering problem is described, putting more emphasis on those new developments of the method necessary to use nonlocal interaction models. In Sec. III, the results for the zero-energy scattering lengths and low-energy elastic-scattering observables are presented and discussed. Some concluding remarks are given in Sec. IV.

II. FORMALISM

In this section we present the HH method for scattering states. The method for bound states has been most recently reviewed in Ref. [10], and its main characteristics are briefly summarized in the following subsection.

A. The HH method for bound states

The nuclear wave function for the three-body system with total angular momentum J, J_z can be written as

$$|\Psi^{JJ_z}\rangle = \sum_\mu c_\mu \big|\Psi_\mu^{JJ_z}\big\rangle, \tag{2.1}$$

where $|\Psi_\mu^{JJ_z}\rangle$ is a suitable complete set of states and μ is an index denoting the set of quantum numbers necessary to completely specify the basis elements.

The coefficients of the expansion can be calculated using the Rayleigh-Ritz variational principle, which states that

$$\langle \delta_c \Psi^{JJ_z} | H - E | \Psi^{JJ_z}\rangle = 0, \tag{2.2}$$

where $\delta_c \Psi^{JJ_z}$ indicates the variation of Ψ^{JJ_z} for arbitrary infinitesimal changes of the linear coefficients c_μ. The problem of determining c_μ and the energy E is then reduced to a generalized eigenvalue problem,

$$\sum_{\mu'} \big\langle \Psi_\mu^{JJ_z} \big| H - E \big| \Psi_{\mu'}^{JJ_z} \big\rangle c_{\mu'} = 0. \tag{2.3}$$

The main difficulty of the method is to compute the matrix elements of the Hamiltonian H with respect to the basis states $|\Psi_\mu^{JJ_z}\rangle$. Usually H is given as a sum of terms (kinetic energy, two-body potential, etc.). The calculation of the matrix elements of some parts of H can be more conveniently performed in coordinate space, while for other parts it could be easier to work in momentum space. Therefore, it is important that the basis states $|\Psi_\mu^{JJ_z}\rangle$ have simple expressions in both spaces. The HH functions indeed have such a property.

Let us first consider the expression of the HH functions in coordinate space. The internal dynamics of a system of three nucleons of identical mass m is conveniently described in terms of the Jacobi vectors $\boldsymbol{x}_{1p}, \boldsymbol{x}_{2p}$, constructed from a given particle permutation denoted with p, which specifies the particle order i, j, k, and given by

$$\begin{aligned} \boldsymbol{x}_{2p} &= \frac{1}{\sqrt{2}}(\boldsymbol{r}_j - \boldsymbol{r}_i) \\ \boldsymbol{x}_{1p} &= \sqrt{\frac{2}{3}}\left[\boldsymbol{r}_k - \frac{1}{2}(\boldsymbol{r}_i + \boldsymbol{r}_j)\right]. \end{aligned} \tag{2.4}$$

Here $p = 1$ corresponds to the order 1,2,3. It is convenient to replace the moduli of $\boldsymbol{x}_{2p}$ and $\boldsymbol{x}_{1p}$ with the so-called hyperradius and hyperangle, defined as [17]

$$\rho = \sqrt{\boldsymbol{x}_{1p}^2 + \boldsymbol{x}_{2p}^2} \tag{2.5}$$

$$\tan\phi_p = \frac{x_{1p}}{x_{2p}}. \tag{2.6}$$

Note that ρ does not depend on the particle permutation p. The complete set of hyperspherical coordinates is then given by $\{\rho, \Omega_p^{(\rho)}\}$, with

$$\Omega_p^{(\rho)} = [\hat{\boldsymbol{x}}_{1p}, \hat{\boldsymbol{x}}_{2p}; \phi_p] \tag{2.7}$$

and the suffix (ρ) recalls the use of the coordinate space.

The expansion states $|\Psi_\mu^{JJ_z}\rangle$ of Eq. (2.1) are then given by

$$|\Psi_\mu^{JJ_z(\rho)}\rangle = f_l(\rho)\mathcal{Y}_{\{G\}}[\Omega^{(\rho)}], \tag{2.8}$$

where $f_l(\rho)$ for $l = 1, \ldots M$ is a complete set of hyperradial functions, chosen of the form

$$f_l(\rho) = \gamma^3 \sqrt{\frac{l!}{(l+5)!}}\; L_l^{(5)}(\gamma\rho)\; \mathrm{e}^{-\frac{\gamma}{2}\rho}. \tag{2.9}$$

Here $L_l^{(5)}(\gamma\rho)$ are Laguerre polynomials, and the nonlinear parameter γ is variationally optimized. As an example, for the N3LO-Idaho potential, it can be chosen in the interval 6–8 fm^{-1}.

The functions $\mathcal{Y}_{\{G\}}[\Omega^{(\rho)}]$ are written as

$$\begin{aligned} \mathcal{Y}_{\{G\}}[\Omega^{(\rho)}] = \sum_{p=1}^{3} \Bigg[Y_{[G]}^{LL_z}\big[\Omega_p^{(\rho)}\big] \otimes \Big[S_2 \otimes \frac{1}{2} \Big]_{SS_z} \Bigg]_{JJ_z} \\ \times \Big[T_2 \otimes \frac{1}{2} \Big]_{TT_z}, \end{aligned} \tag{2.10}$$

where the sum is performed over the three even permutations. The spins (isospins) of particle i and j are coupled to S_2 (T_2), which is itself coupled to the spin (isospin) of the third particle to give the state with total spin S (isospin T, T_z). The total orbital angular momentum L and the total spin S are coupled to the total angular momentum J, J_z. The functions $Y_{[G]}^{LL_z}[\Omega_p^{(\rho)}]$, having a definite value of L, L_z, are the HH functions and are written as [13]:

$$\begin{aligned} &Y_{[G]}^{LL_z}\big[\Omega_p^{(\rho)}\big] \\ &\quad = [Y_{\ell_2}(\hat{\boldsymbol{x}}_{2p}) \otimes Y_{\ell_1}(\hat{\boldsymbol{x}}_{1p})]_{LL_z} N_{[G]} (\cos\phi_p)^{\ell_2} (\sin\phi_p)^{\ell_1} \\ &\qquad \times P_n^{\ell_1+\frac{1}{2},\ell_2+\frac{1}{2}}(\cos 2\phi_p). \end{aligned} \tag{2.11}$$

Here $Y_{\ell_1}(\hat{\boldsymbol{x}}_{1p})$ and $Y_{\ell_2}(\hat{\boldsymbol{x}}_{2p})$ are spherical harmonics, $N_{[G]}$ is a normalization factor and $P_n^{\ell_1+\frac{1}{2},\ell_2+\frac{1}{2}}(\cos 2\phi_p)$ is a Jacobi polynomial, n being the degree of the polynomial. The grand angular quantum number G is defined as $G = 2n + \ell_1 + \ell_2$. The notations $[G]$ and $\{G\}$ of Eqs. (2.11) and (2.10) stand for $[\ell_1, \ell_2; n]$ and $\{\ell_1, \ell_2, L, S_2, T_2, S, T; n\}$, respectively, and μ of Eq. (2.8) is $\mu = \{G\}, l$. Note that each set of quantum numbers $\{\ell_1, \ell_2, L, S_2, T_2, S, T\}$ is called "channel," and the antisymmetrization of $\mathcal{Y}_{\{G\}}[\Omega^{(\rho)}]$ requires $\ell_2 + S_2 + T_2$ to be odd. In addition, $\ell_1 + \ell_2$ must be even (odd) for positive (negative) parity. To be noticed that after the sum on the permutation in Eq. (2.10), some states inside the subspace spanned by G are linearly dependent. These states have been identified and removed from the expansion [10,13].

In this work, we have considered modern two-body potential models that act on specific spin and angular-momentum states of the two-body system. Due to the presence of the sum over the permutations in the expression for $\mathcal{Y}_{\{G\}}$, a given particle pair is not in a definite angular and spin state. However, the HH functions with the grand angular quantum number G constructed in terms of a given set of Jacobi vectors $\boldsymbol{x}_{1p}, \boldsymbol{x}_{2p}$, defined starting from the particle order i, j, k, can be always expressed in terms of the HH functions constructed, for instance, in terms of $\boldsymbol{x}_{1(p=1)}, \boldsymbol{x}_{2(p=1)}$. In fact, the following relation holds

$$Y^{LL_z}_{[\ell_1,\ell_2;n]}\left[\Omega^{(\rho)}_p\right] = \sum_{\ell_1',\ell_2',n'} a^{(p),L}_{\ell_1,\ell_2,n;\ell_1',\ell_2',n'} Y^{LL_z}_{[\ell_1',\ell_2';n']}\left[\Omega^{(\rho)}_{(p=1)}\right], \tag{2.12}$$

where the sum is restricted to the values ℓ_1', ℓ_2', and n' such that $\ell_1' + \ell_2' + 2n' = G$. The coefficients $a^{(p),L}_{\ell_1,\ell_2,n;\ell_1',\ell_2',n'}$ relating the two sets of HH functions are known as the Raynal-Revai coefficients [18] and could be computed rather easily using the orthonormality property of the HH functions, namely

$$a^{(p),L}_{\ell_1,\ell_2,n;\ell_1',\ell_2',n'} = \int d\Omega^{(\rho)}_{(p=1)} \left\{Y^{LL_z}_{[\ell_1,\ell_2;n]}\left[\Omega^{(\rho)}_{(p=1)}\right]\right\}^* Y^{LL_z}_{[\ell_1',\ell_2';n']}\left[\Omega^{(\rho)}_p\right]. \tag{2.13}$$

Also the spin-isospin states can be recoupled to obtain states where the spin and isospin quantum numbers are coupled in a given order of the particles. The result is that the antisymmetric functions $\mathcal{Y}_{\{G\}}$ can be expressed as a superposition of functions constructed in terms of a given order of particles i, j, k, each one having the pair i,j in a definite spin and angular momentum state. When the two-body potential acts on the pair of particles i,j, the effect of the projection is easily taken into account.

The expansion states of Eq. (2.1) in momentum space can be obtained as follows. Let $\hbar\boldsymbol{k}_{1p}, \hbar\boldsymbol{k}_{2p}$ be the conjugate Jacobi momenta of the Jacobi vectors, given by

$$\begin{aligned} \hbar\boldsymbol{k}_{2p} &= \frac{1}{\sqrt{2}}(\boldsymbol{p}_j - \boldsymbol{p}_i) \\ \hbar\boldsymbol{k}_{1p} &= \sqrt{\frac{2}{3}}\left[\boldsymbol{p}_k - \frac{1}{2}(\boldsymbol{p}_i + \boldsymbol{p}_j)\right], \end{aligned} \tag{2.14}$$

$\boldsymbol{p}_i$ being the momentum of the i-th particle. We then define a hypermomentum Q and a set of angular-hyperangular variables as

$$\begin{aligned} Q &= \sqrt{\boldsymbol{k}_{1p}^2 + \boldsymbol{k}_{2p}^2} \\ \Omega^{(Q)}_p &= [\hat{\boldsymbol{k}}_{2p}, \hat{\boldsymbol{k}}_{1p}; \varphi_p], \end{aligned} \tag{2.15}$$

where

$$\tan\varphi_p = \frac{k_{1p}}{k_{2p}}. \tag{2.16}$$

Then, the momentum-space version of the wave function given in Eq. (2.8) is

$$\left|\Psi^{JJ_z(Q)}_{\mu}\right\rangle = g_{G,l}(Q)\mathcal{Y}_{\{G\}}[\Omega^{(Q)}], \tag{2.17}$$

where $\mathcal{Y}_{\{G\}}[\Omega^{(Q)}]$ is the same as $\mathcal{Y}_{\{G\}}[\Omega^{(\rho)}]$ of Eq. (2.10) with $\boldsymbol{x}_{ip} \to \boldsymbol{k}_{ip}$, and

$$g_{G,l}(Q) = (-i)^G \int_0^\infty d\rho \, \frac{\rho^3}{Q^2} \, J_{G+2}(Q\rho) \, f_l(\rho). \tag{2.18}$$

With the adopted form of $f_l(\rho)$ given in Eq. (2.9), the corresponding functions $g_{G,l}(Q)$ can be easily calculated, and they are explicitly given in Ref. [15].

B. The HH method for scattering states below deuteron breakup threshold

We consider here the extension of the HH technique to describe N-d scattering states below deuteron breakup threshold, when both local and nonlocal interaction models are considered.

Following Ref. [12], the wave function $\Psi^{LSJJ_z}_{N\text{-}d}$ describing the N-d scattering state with incoming orbital angular momentum L and channel spin S, parity $\pi = (-)^L$, and total angular momentum J, J_z, can be written as

$$\Psi^{LSJJ_z}_{N\text{-}d} = \Psi^{LSJJ_z}_C + \Psi^{LSJJ_z}_A, \tag{2.19}$$

where $\Psi^{LSJJ_z}_C$ describes the system in the region where the particles are close to each other and their mutual interactions are strong, while $\Psi^{LSJJ_z}_A$ describes the relative motion between the nucleon N and the deuteron in the asymptotic region, where the N-d nuclear interaction is negligible. The function $\Psi^{LSJJ_z}_C$, which has to vanish in the limit of large intercluster separations, can be expanded on the HH basis as it has been done in the case of bound states. Therefore, applying Eq. (2.1), the function $\Psi^{LSJJ_z}_C$ can be casted in the form

$$\left|\Psi^{LSJJ_z}_C\right\rangle = \sum_\mu c_\mu \left|\Psi^{JJ_z}_\mu\right\rangle, \tag{2.20}$$

where $|\Psi^{JJ_z}_\mu\rangle$ is defined in Eqs. (2.8) and (2.17) in coordinate and momentum space, respectively.

The function $\Psi^{LSJJ_z}_A$ is the appropriate asymptotic solution of the relative N-d Schrödinger equation. It is written as a

linear combination of the following functions,

$$\Omega^{\lambda}_{LSJJ_z} = \sum_{p=1}^{3} \Omega^{\lambda}_{LSJJ_z}(p), \tag{2.21}$$

where the sum over p has to be done over the three even permutations necessary to antisymmetrize the functions $\Omega^{\lambda}_{LSJJ_z}$ and

$$\Omega^{\lambda}_{LSJJ_z}(p) = \sum_{l=0,2} w_l(x_{2p})\, R^{\lambda}_L(y_p) \Big\{ \Big[[Y_l(\hat{\boldsymbol{x}}_{2p}) \otimes S_2]_1 \otimes \frac{1}{2} \Big]_S \otimes Y_L(\hat{\boldsymbol{y}}_p) \Big\}_{JJ_z} \Big[T_2 \otimes \frac{1}{2} \Big]_{TT_z}. \tag{2.22}$$

Here the spin and isospin quantum numbers of particles i and j have been coupled to S_2 and T_2, with $S_2 = 1$, $T_2 = 0$ for the deuteron, $w_l(x_{2p})$ is the deuteron wave function component in the waves $l = 0, 2$, $\boldsymbol{y}_p$ is the distance between N and the center of mass of the deuteron, i.e., $\boldsymbol{y}_p = \sqrt{\frac{3}{2}}\boldsymbol{x}_{1p}$, $Y_l(\hat{\boldsymbol{x}}_{2p})$ and $Y_L(\hat{\boldsymbol{y}}_p)$ are the standard spherical harmonic functions, and the functions $R^{\lambda}_L(y_p)$ are the regular ($\lambda \equiv R$) and irregular ($\lambda \equiv I$) radial solutions of the relative two-body N-d Schrödinger equation without the nuclear interaction. These regular and irregular functions, denoted as $\mathcal{F}_L(y_p)$ and $\mathcal{G}_L(y_p)$, respectively, have the form

$$R^R_L(y_p) \equiv \mathcal{F}_L(y_p) = \frac{1}{(2L+1)!!q^L C_L(\eta)} \frac{F_L(\eta, \xi_p)}{\xi_p}$$

$$R^I_L(y_p) \equiv \mathcal{G}_L(y_p) = (2L+1)!!q^{L+1} C_L(\eta) f_R(y_p) \frac{G_L(\eta, \xi_p)}{\xi_p}, \tag{2.23}$$

where q is the modulus of the N-d relative momentum (related to the total kinetic energy in the center-of-mass system by $T_{\text{c.m.}} = \frac{q^2}{2\mu}$, μ being the N-d reduced mass), $\eta = 2\mu e^2/q$ and $\xi_p = q y_p$ are the usual Coulomb parameters, and the regular (irregular) Coulomb function $F_L(\eta, \xi_p)$ [$G_L(\eta, \xi_p)$] and the factor $C_L(\eta)$ are defined in the standard way [19]. The factor $(2L+1)!!q^L C_L(\eta)$ has been introduced so that $\mathcal{F}$ and $\mathcal{G}$ have a finite limit for $q \to 0$. The function $f_R(y_p) = [1 - \exp(-b y_p)]^{2L+1}$ has been introduced to regularize G_L at small values of y_p. The trial parameter b is determined by requiring that $f_R(y_p) \to 1$ for large values of y_p, thus not modifying the asymptotic behavior of the scattering wave function. A value of $b = 0.25$ fm^{-1} has been found appropriate. The non-Coulomb case of Eq. (2.23) is obtained in the limit $e^2 \to 0$. In this case, $F_L(\eta, \xi_p)/\xi_p$ and $G_L(\eta, \xi_p)/\xi_p$ reduce to the regular and irregular Riccati-Bessel functions and the factor $(2L+1)!!C_L(\eta) \to 1$ for $\eta \to 0$.

With the above definitions, $\Psi^{LSJJ_z}_A$ can be written in the form

$$\Psi^{LSJJ_z}_A = \sum_{L'S'} \left[\delta_{LL'}\delta_{SS'} \Omega^R_{L'S'JJ_z} + \mathcal{R}^J_{LS,L'S'}(q) \Omega^I_{L'S'JJ_z} \right], \tag{2.24}$$

where the parameters $\mathcal{R}^J_{LS,L'S'}(q)$ give the relative weight between the regular and irregular components of the wave function. They are closely related to the reactance matrix ($\mathcal{K}$-matrix) elements, which can be written as

$$\mathcal{K}^J_{LS,L'S'}(q) = (2L+1)!!(2L'+1)!!q^{L+L'+1} \times C_L(\eta) C_{L'}(\eta) \mathcal{R}^J_{LS,L'S'}(q). \tag{2.25}$$

By definition of the $\mathcal{K}$ matrix, its eigenvalues are $\tan\delta_{LSJ}$, δ_{LSJ} being the phase shifts. The sum over L' and S' in Eq. (2.24) is over all values compatible with a given J and parity π. In particular, the sum over L' is limited to include either even or odd values, because $(-1)^{L'} = \pi$.

The matrix elements $\mathcal{R}^J_{LS,L'S'}(q)$ and the linear coefficients c_μ occurring in the expansion of $\Psi^{LSJJ_z}_C$ of Eq. (2.20) are determined applying the Kohn variational principle [20], which states that the functional

$$\left[\mathcal{R}^J_{LS,L'S'}(q)\right] = \mathcal{R}^J_{LS,L'S'}(q) - \left\langle \Psi^{L'S'JJ_z}_{N\text{-}d} \right| \mathcal{L} \left| \Psi^{LSJJ_z}_{N\text{-}d} \right\rangle$$

$$\mathcal{L} = \frac{m}{2\sqrt{3}\hbar^2}(H - E) \tag{2.26}$$

has to be stationary with respect to variations of the trial parameters in $\Psi^{LSJJ_z}_{N\text{-}d}$. Here E is the total energy of the system, m is the nucleon mass, and $\mathcal{L}$ is chosen so that

$$\left\langle \Omega^R_{LSJJ_z} \middle| \mathcal{L} \middle| \Omega^I_{LSJJ_z} \right\rangle - \left\langle \Omega^I_{LSJJ_z} \middle| \mathcal{L} \middle| \Omega^R_{LSJJ_z} \right\rangle = 1. \tag{2.27}$$

As described in Ref. [21], using Eqs. (2.20) and (2.24), the variation of the diagonal functionals of Eq. (2.26) with respect to the linear parameters c_μ leads to the following system of linear inhomogeneous equations:

$$\sum_{\mu'} \left\langle \Psi^{JJ_z}_{\mu} \middle| \mathcal{L} \middle| \Psi^{JJ_z}_{\mu'} \right\rangle c_{\mu'} = -D^{\lambda}_{LSJJ_z}(\mu). \tag{2.28}$$

Two different terms D^{λ} corresponding to $\lambda \equiv R, I$ are introduced and are defined as

$$D^{\lambda}_{LSJJ_z}(\mu) = \left\langle \Psi^{JJ_z}_{\mu} \middle| \mathcal{L} \middle| \Omega^{\lambda}_{LSJJ_z} \right\rangle. \tag{2.29}$$

The matrix elements $\mathcal{R}^J_{LS,L'S'}(q)$ are obtained varying the diagonal functionals of Eq. (2.26) with respect to them. This leads to the following set of algebraic equations

$$\sum_{L''S''} \mathcal{R}^J_{LS,L''S''}(q) X_{L'S',L''S''} = Y_{LS,L'S'} \tag{2.30}$$

with the coefficients X and Y defined as

$$X_{LS,L'S'} = \left\langle \Omega^I_{LSJJ_z} + \Psi^{LSJJ_z,I}_C \middle| \mathcal{L} \middle| \Omega^I_{L'S'JJ_z} \right\rangle$$
$$Y_{LS,L'S'} = -\left\langle \Omega^R_{LSJJ_z} + \Psi^{LSJJ_z,R}_C \middle| \mathcal{L} \middle| \Omega^I_{L'S'JJ_z} \right\rangle. \tag{2.31}$$

Here $\Psi^{LSJJ_z,\lambda}_C$ is the solution of the set of Eq. (2.28) with the corresponding D^{λ} term. A second-order estimate of $\mathcal{R}^J_{LS,L'S'}(q)$ is given by the quantities $[\mathcal{R}^J_{LS,L'S'}(q)]$, obtained by substituting in Eq. (2.26) the first order results. Such second-order calculation provides a symmetric reactance matrix. This condition is not *a priori* imposed, and therefore it is a useful test of the numerical accuracy.

In the particular case of $q = 0$ (zero-energy scattering), the scattering can occur only in the channel $L = 0$ and the

observables of interest are the scattering lengths. Within the present approach, they can be easily obtained from the relation

$$^{(2J+1)}a_{Nd} = -\lim_{q\to 0} \mathcal{R}^J_{0J,0J}(q). \tag{2.32}$$

An alternative way to solve the scattering problem, used when $q \neq 0$, is to apply the complex Kohn variational principle to the $\mathcal{S}$ matrix, as in Ref. [21]. In this way, the Kohn variational principle of Eq. (2.26) becomes

$$\left[\mathcal{S}^J_{LS,L'S'}(q)\right] = \mathcal{S}^J_{LS,L'S'}(q) + i\left\langle \Psi^{+,L'S'JJ_z}_{N\text{-}d} \middle| \mathcal{S} \middle| \Psi^{+,LSJJ_z}_{N\text{-}d} \right\rangle. \tag{2.33}$$

Here

$$\Psi^{+,LSJJ_z}_{N\text{-}d} = \Psi^{LSJJ_z}_C + \Psi^{+,LSJJ_z}_A \tag{2.34}$$

with $\Psi^{LSJJ_z}_C$ given in Eq. (2.20) and

$$\begin{aligned}\Psi^{+,LSJJ_z}_A &= \sum_{p=1}^{3} \Omega^+_{LSJJ_z}(p)\\ \Omega^+_{LSJJ_z}(p) &= \left[i\tilde{\Omega}^R_{LSJJ_z}(p) - \tilde{\Omega}^I_{LSJJ_z}(p)\right]\\ &\quad + \sum_{L'S'} \mathcal{S}^J_{LS,L'S'}(q)\left[i\tilde{\Omega}^R_{L'S'JJ_z}(p) + \tilde{\Omega}^I_{L'S'JJ_z}(p)\right].\end{aligned} \tag{2.35}$$

The functions $\tilde{\Omega}^\lambda_{LSJJ_z}(p)$ are the same as in Eq. (2.22), with $R^R_L(y_p) = F_L(\eta,\xi_p)/\xi_p$ and $R^I_L(y_p) = f_R(y_p)G_L(\eta,\xi_p)/\xi_p$. Note that, with the above definition, the reactance $\mathcal{K}$-matrix elements can be related to the $\mathcal{S}$-matrix elements as

$$\begin{aligned}\mathcal{K}^J_{LS,L'S'}(q) &= (-i)\left[\mathcal{S}^J_{LS,L'S'}(q) - \delta_{LL'}\delta_{SS'}\right]\\ &\quad \times \left[\mathcal{S}^J_{LS,L'S'}(q) + \delta_{LL'}\delta_{SS'}\right]^{-1}.\end{aligned} \tag{2.36}$$

The calculation involving $\Psi^{LSJJ_z}_C$ has been performed with the HH expansion in coordinate or in momentum space, depending on what is more convenient, as it has been explained for the bound state in the previous subsection. Some difficulties arise for the calculation of the potential energy matrix elements that involve $\Omega^\lambda_{LSJJ_z}$, i.e., $\langle\Psi^{JJ_z}_\mu|V|\Omega^\lambda_{LSJJ_z}\rangle$ present in Eq. (2.29), and $\langle\Omega^{\lambda'}_{L'S'JJ_z} + \Psi^{L'S'JJ_Z,\lambda'}_C|V|\Omega^\lambda_{LSJJ_z}\rangle$ of Eq. (2.31), with $\lambda, \lambda' = R, I$. In the present work, we consider both two- and three-nucleon interactions, and therefore

$$V = \sum_{i<j} V_{ij} + \sum_{i<j<k} V_{ijk}. \tag{2.37}$$

We first focus on the two-body contribution. Due to the antisymmetry of the wave function, the following relation holds

$$\langle\Phi|\sum_{i<j} V_{ij}|\Omega^\lambda_{LSJJ_z}(p)\rangle = 3\langle\Phi|V_{12}|\Omega^\lambda_{LSJJ_z}(p)\rangle, \tag{2.38}$$

where $|\Phi\rangle$ can be either $|\Psi^{JJ_z}_\mu\rangle$ of Eq. (2.20) or $\Omega^{\lambda'}_{L'S'JJ_z}(p')$ of Eq. (2.22), depending on which term among D^λ, X, and Y is considered. The potential V_{12} acts on the particle pair 1,2 with total angular momentum j, and orbital angular momentum and spin quantum numbers ℓ'_{12}, s'_{12} (on the bra) and ℓ_{12}, s_{12} (on the ket), and can be written as

$$V_{12} = v^j_{12}[x'_{2\,(p=1)}, x_{2\,(p=1)}; \ell'_{12}, s'_{12}, \ell_{12}, s_{12}], \tag{2.39}$$

in coordinate space and

$$V_{12} = v^j_{12}[k'_{2\,(p=1)}, k_{2\,(p=1)}; \ell'_{12}, s'_{12}, \ell_{12}, s_{12}], \tag{2.40}$$

in momentum space, where $x_{2\,(p=1)}$ and $k_{2\,(p=1)}$ are the moduli of the vectors defined in Eqs. (2.4) and (2.14), respectively. When local potential models are considered, such as the AV18, then

$$\begin{aligned}&v^j_{12}[x'_{2\,(p=1)}, x_{2\,(p=1)}; \ell'_{12}, s'_{12}, \ell_{12}, s_{12}]\\ &\quad \to v^j_{12}[x_{2\,(p=1)}; \ell'_{12}, s'_{12}, \ell_{12}, s_{12}]\delta[x_{2\,(p=1)} - x'_{2\,(p=1)}].\end{aligned} \tag{2.41}$$

The first difficulty that needs to be overcame arises from the fact that when the V_{12} operator acts on $\Omega^\lambda_{LSJJ_z}(p \neq 1)$, the particle pair 12 does not have a well-definined orbital and spin angular momenta. However, the following relation holds:

$$\begin{aligned}&w_l[x_{2(p\neq1)}]\, R^\lambda_L(y_{p\neq1})[Y_l(\hat{\boldsymbol{x}}_{2(p\neq1)}) \otimes Y_L(\hat{\boldsymbol{y}}_{p\neq1})]_{\Lambda,\Lambda_z}\\ &\quad = \sum_{l',L'} F^{\lambda,p\neq1}_{lL;l'L'}[x_{1\,(p=1)}, x_{2\,(p=1)}]\\ &\qquad \times \left[Y_{l'}(\hat{\boldsymbol{x}}_{2(p=1)}) \otimes Y_{L'}(\hat{\boldsymbol{y}}_{p=1})\right]_{\Lambda,\Lambda_z}.\end{aligned} \tag{2.42}$$

where Λ, Λ_z are the total orbital angular momentum and its third component. The functions $F^{\lambda,p\neq1}_{lL;l'L'}[x_{1(p=1)}, x_{2(p=1)}]$ are given by

$$\begin{aligned}&F^{\lambda,p\neq1}_{lL;l'L'}[x_{1(p=1)}, x_{2(p=1)}]\\ &\quad = \int d\hat{\boldsymbol{x}}_{2(p=1)} d\hat{\boldsymbol{x}}_{1(p=1)}\left[Y^*_{l'}(\hat{\boldsymbol{x}}_{2(p=1)}) \otimes Y^*_{L'}(\hat{\boldsymbol{y}}_{p=1})\right]_{\Lambda,\Lambda_z}\\ &\qquad \times w_l[x_{2(p\neq1)}]\, R^\lambda_L(y_{p\neq1})\left[Y_l(\hat{\boldsymbol{x}}_{2(p\neq1)}) \otimes Y_L(\hat{\boldsymbol{y}}_{p\neq1})\right]_{\Lambda,\Lambda_z}.\end{aligned} \tag{2.43}$$

Once the functions $F^{\lambda,p\neq1}_{lL;l'L'}[x_{1(p=1)}, x_{2(p=1)}]$ have been calculated and the spin-isospin states have been also properly recoupled, the effect of the projection operator in V_{12} is easily taken into account.

A second difficulty arises in the calculation of the potential matrix element, when nonlocal potentials expressed in momentum space are used. On the contrary to the core part of the scattering wave function $\Psi^{LSJJ_z}_C$, which can be alternatively expressed in coordinate or in momentum space, the asymptotic states $\Omega^\lambda_{LSJJ_z}$ have no easy expression in momentum space and are more conveniently expressed and used in coordinate space. This is especially true when the Coulomb interaction is considered, as for the p-d case. Therefore, we have decided to perform the Fourier transform of the potential $v^j_{12}(k', k; \ell', s', \ell, s)$ to work only in coordinate space, namely

$$\begin{aligned}&v^j_{12}(r', r; \ell', s', \ell, s)\\ &\quad = \frac{2}{\pi}\int k^2 dk\; k'^2 dk'\; j_{\ell'}(k'r')\, v^j_{12}(k', k; \ell', s', \ell, s)\, j_\ell(kr),\end{aligned} \tag{2.44}$$

where $j_\ell(kr)$ and $j_{\ell'}(k'r')$ are the standard spherical Bessel functions. The integrations over k and k', which run from 0 to

∞, are easily performed when the potential model considered does not have a high-momentum tail but goes rapidly to zero at rather low values of k and k'. This is true for the N3LO-Idaho and $V_{\text{low-}k}$ potential models but not for the CDBonn. Because the main goal of the present work is to perform a first test of the applicability of the HH method to the $A = 3$ scattering problem using nonlocal realistic interactions, only the N3LO-Idaho and $V_{\text{low-}k}$ two-body potentials have been considered.

Some remarks about the calculation of the three-body contribution to the potential energy operator of Eq. (2.37) are in order. The TNIs considered in the present work are the Urbana IX [5] (UIX) and the N2LO [7] potentials. The first one is used in conjunction with both the AV18 and N3LO-Idaho two-nucleon interactions. In the second case, the parameter in front of the spin-isospin independent part of the UIX TNI has been rescaled by a factor of 0.384 to fit the triton binding energy [22] (UIXp). The N2LO TNI has been used only in conjunction with the N3LO-Idaho potential model. All these TNIs are local potentials, and have a well-defined operatorial structure. Therefore, the projection procedure of Eqs. (2.42) and (2.43) is not needed and the present approach follows the footsteps of the PHH technique [12,23].

III. RESULTS

In this section we present our results for n-d and p-d scattering observables at center-of-mass energies below deuteron breakup threshold. The interaction models that have been used are the AV18 and the N3LO-Idaho two-nucleon interactions and the AV18/UIX, N3LO-Idaho/UIXp, and the N3LO-Idaho/N2LO two- and three-nucleon interactions. Note that the AV18 and AV18/UIX results are the same as those ones first obtained in Ref. [24], using the PHH expansion. We have considered also the $V_{\text{low-}k}$ model, obtained from the AV18 two-nucleon interaction with a cutoff parameter Λ equal to 2.2 fm^{-1}. The cutoff parameter has been chosen so that the triton binding energy is 8.477 MeV, when the complete electromagnetic interaction is used, including neutron charge distribution and MM interaction effects. However, when no electromagnetic effects are considered, the triton binding energy has been found to be 8.519 MeV. In the scattering problem, only the point Coulomb interaction has been considered, except when differently indicated.

Before presenting the results for the considered low-energy N-d observables, we discuss the pattern of convergence for some representative quantities, i.e. the n-d doublet zero-energy scattering length $^2a_{nd}$ and the p-d $J^\pi = 1/2^+, 1/2^-$ phase shifts and mixing angles at center-of-mass energy $E_{\text{c.m.}} = 2.0$ MeV, calculated with the N3LO-Idaho two-nucleon interaction model. The angular momentum-spin-isospin channels considered for $J^\pi = 1/2^+$ and $1/2^-$ are given in Tables I and II, respectively. The notation is the same as in Eq. (2.11). To be noticed that the scattering channels in the case of $J^\pi = 1/2^-$ are ordered for increasing values of $\ell_1 + \ell_2$. This is true also for all the channels here considered, except those for $J^\pi = 1/2^+$ (see Table I), where the ordering respects a "historical choice," first done in the case of the three-nucleon bound state in Ref. [25].

TABLE I. Angular-momentum, spin, and isospin quantum numbers for the first 23 channels considered in the expansion of the $J^\pi = 1/2^+$ core wave function.

α	$\ell_{1\alpha}$	$\ell_{2\alpha}$	L_α	$S_{2\alpha}$	$T_{2\alpha}$	S_α	T_α
1	0	0	0	1	0	1/2	1/2
2	0	0	0	0	1	1/2	1/2
3	0	2	2	1	0	3/2	1/2
4	2	0	2	1	0	3/2	1/2
5	2	2	0	1	0	1/2	1/2
6	2	2	2	1	0	3/2	1/2
7	2	2	1	1	0	1/2	1/2
8	2	2	1	1	0	3/2	1/2
9	1	1	0	1	1	1/2	1/2
10	1	1	1	1	1	1/2	1/2
11	1	1	1	1	1	3/2	1/2
12	1	1	2	1	1	3/2	1/2
13	1	1	0	0	0	1/2	1/2
14	1	1	1	0	0	1/2	1/2
15	2	2	0	0	1	1/2	1/2
16	2	2	1	0	1	1/2	1/2
17	3	1	2	1	1	3/2	1/2
18	1	3	2	1	1	3/2	1/2
19	0	0	0	0	1	1/2	3/2
20	1	1	0	1	1	1/2	3/2
21	1	1	1	1	1	1/2	3/2
22	1	1	1	1	1	3/2	3/2
23	1	1	2	1	1	3/2	3/2

TABLE II. Same as in Table I but for the first 25 channels considered in the expansion of the $J^\pi = 1/2^-$ core wave function.

α	$\ell_{1\alpha}$	$\ell_{2\alpha}$	L_α	$S_{2\alpha}$	$T_{2\alpha}$	S_α	T_α
1	1	0	1	1	0	1/2	1/2
2	1	0	1	0	1	1/2	1/2
3	1	0	1	1	0	3/2	1/2
4	0	1	1	1	1	1/2	1/2
5	0	1	1	0	0	1/2	1/2
6	0	1	1	1	1	3/2	1/2
7	2	1	1	1	1	1/2	1/2
8	2	1	1	0	0	1/2	1/2
9	2	1	1	1	1	3/2	1/2
10	2	1	2	1	1	3/2	1/2
11	1	2	1	1	0	1/2	1/2
12	1	2	1	0	1	1/2	1/2
13	1	2	1	1	0	3/2	1/2
14	1	2	2	1	0	3/2	1/2
15	3	2	1	1	0	1/2	1/2
16	3	2	1	0	1	1/2	1/2
17	3	2	1	1	0	3/2	1/2
18	3	2	2	1	0	3/2	1/2
19	1	0	1	0	1	1/2	3/2
20	0	1	1	1	1	1/2	3/2
21	0	1	1	1	1	3/2	3/2
22	2	1	1	1	1	1/2	3/2
23	2	1	1	1	1	3/2	3/2
24	2	1	2	1	1	3/2	3/2
25	1	2	1	0	1	1/2	3/2

TABLE III. n-d doublet scattering length ${}^2a_{nd}$ in fm and p-d $J^\pi = 1/2^+, 1/2^-$ phase shifts δ_{LSJ} and mixing angles ϵ at $E_{\rm c.m.} = 2.0$ MeV, calculated with the HH technique using the N3LO-Idaho interaction model, for increasing values of the Laguerre polynomials M. All the channels of Tables I and II are included with grand angular momentum for all the channels set equal to 20 for $J^\pi = 1/2^+$ and 21 for $J^\pi = 1/2^-$.

	$M = 4$	$M = 8$	$M = 12$	$M = 16$	$M = 20$	$M = 24$	$M = 28$
${}^2a_{nd}$	3.029	1.630	1.329	1.259	1.240	1.234	1.233
$\delta_{0,\frac{1}{2},\frac{1}{2}}$	−3.611	−3.583	−3.572	−3.570	−3.570	−3.569	−3.569
$\delta_{2,\frac{3}{2},\frac{1}{2}}$	−43.28	−34.69	−32.41	−31.96	−31.82	−31.78	−31.77
$\epsilon_{\frac{1}{2}^+}$	0.525	0.975	1.150	1.189	1.201	1.205	1.206
$\delta_{1,\frac{1}{2},\frac{1}{2}}$	−8.270	−7.756	−7.608	−7.581	−7.576	−7.575	−7.575
$\delta_{1,\frac{3}{2},\frac{1}{2}}$	20.82	21.73	21.97	22.00	22.00	22.01	22.01
$\epsilon_{\frac{1}{2}^-}$	4.947	5.542	5.628	5.641	5.643	5.644	5.644

In Table III we present the results for ${}^2a_{nd}$ and p-d $J^\pi = 1/2^+, 1/2^-$ phase shifts and mixing angles (δ_{LSJ}, ϵ) at $E_{\rm c.m.} = 2.0$ MeV for increasing values of the Laguerre polynomials M in the hyperradial functions [see Eqs. (2.9) and (2.18)]. All the 23 (25) angular momentum-spin-isospin channels of Table I (II) are considered for $J^\pi = 1/2^+$ $(1/2^-)$, and HH functions up to grand angular momentum $G = 20\,(21)$ for all the channels have been included. From inspection of the table, we can conclude that the use of $M = 28$ is enough to reach an accuracy of at least 0.002 fm for the scattering length and four significant digits for the phase shifts and mixing angles. In fact, for other p-d scattering channels at some of the considered values of $E_{\rm c.m.}$, even $M = 24$ and $M = 20$ has been found enough to reach the same degree of accuracy.

To study the convergence on the HH expansion, as it has been done in Ref. [14], we have separated the HH functions into classes having particular properties and we have taken into account the fact that the convergence rates of the different classes are rather different. For instance, we expect that the contribution of the HH functions with lower values of $\ell_{12,\alpha} = \ell_{1,\alpha} + \ell_{2,\alpha}$ to be the most important. Therefore, for all the J^π-scattering states, except $J^\pi = 1/2^+$, the different classes are classified with increasing value of $\ell_{12,\alpha}$, up to $\ell_{12,\alpha} \leqslant 6$, and among those ones with the same $\ell_{12,\alpha}$, we have included first the contributions of the HH functions with lower $\ell_{2,\alpha}$. Finally, the $T_\alpha = 3/2$ states are considered. With these criteria, in the $J^\pi = 1/2^-$ case, the channels have been classified into six classes, including channels 1–3, 4–6, 7–10, 11–14, 15–18, and 19–25 of Table II, respectively. In the case of $J^\pi = 1/2^+$, the classification follows the footsteps of Ref. [25], and therefore the channels have been classified into five classes, including channels 1–3, 4–8, 9–12, 13–18, and 19–23 of Table I, respectively. We have then called G_i, for each class i, a number such that each state of class i has the grand angular momentum $G \leqslant G_i$, and we have increased G_i until we have reached convergence. Then, keeping G_i fixed at this value, we have included the states of the following class and increased G_{i+1} again until we have reached convergence. The results for the zero-energy scattering length and the low-energy phase shifts and mixing angles obtained with this procedure are given in Table IV for $J^\pi = 1/2^+$ and V for $J^\pi = 1/2^-$.

TABLE IV. Convergence of the n-d doublet scattering length ${}^2a_{nd}$ in fm and p-d $J^\pi = 1/2^+$ phase shifts δ_{LSJ} and mixing angles ϵ at $E_{\rm c.m.} = 2.0$ MeV, corresponding to the inclusion in the wave function of the different classes in which the HH basis has been divided. The N3LO-Idaho interaction model is used, and the number of Laguerre polynomials included is $M = 28$.

G_1	G_2	G_3	G_4	G_5	${}^2a_{nd}$	$\delta_{0,\frac{1}{2},\frac{1}{2}}$	$\delta_{2,\frac{3}{2},\frac{1}{2}}$	$\epsilon_{\frac{1}{2}^+}$
50					1.245	−3.577	−32.11	1.248
60					1.243	−3.577	−32.09	1.248
70					1.242	−3.577	−32.08	1.248
80					1.242	−3.577	−32.08	1.248
80	16				1.112	−3.572	−31.18	1.240
80	20				1.112	−3.572	−31.17	1.238
80	20	16			1.100	−3.569	−31.09	1.239
80	20	20			1.100	−3.569	−31.09	1.239
80	20	20	16		1.099	−3.569	−31.09	1.239
80	20	20	20		1.099	−3.569	−31.09	1.239
80	20	20	20	16	1.099	−3.569	−31.04	1.241
80	20	20	20	20	1.099	−3.569	−31.04	1.241

TABLE V. Same as in Table IV but for p-d $J^\pi = 1/2^-$ phase shifts δ_{LSJ} and mixing angles ϵ at $E_{\rm c.m.} = 2.0$ MeV.

G_1	G_2	G_3	G_4	G_5	G_6	$\delta_{1,\frac{1}{2},\frac{1}{2}}$	$\delta_{1,\frac{3}{2},\frac{1}{2}}$	$\epsilon_{\frac{1}{2}^-}$
61						−7.416	21.24	5.544
71						−7.413	21.25	5.545
81						−7.412	21.25	5.545
91						−7.411	21.25	5.545
91	11					−7.382	21.53	5.619
91	21					−7.380	21.55	5.622
91	31					−7.379	21.55	5.622
91	31	15				−7.367	21.77	5.704
91	31	21				−7.367	21.77	5.705
91	31	21	31			−7.372	22.02	5.799
91	31	21	41			−7.370	22.03	5.798
91	31	21	51			−7.369	22.04	5.798
91	31	21	51	15		−7.369	22.04	5.798
91	31	21	51	21		−7.369	22.04	5.798
91	31	21	51	21	15	−7.342	22.05	5.818
91	31	21	51	21	21	−7.340	22.05	5.819

Here, $M = 28$ Laguerre polynomials in the expansion of the hyperradial function are included and again the N3LO-Idaho two-nucleon potential is used.

From the cases presented in the tables, and as well as for all cases taken in consideration, we can observe that (i) the last classes of channels, corresponding to the $T_\alpha = 3/2$ states, give sizable contributions to the p-d phase shifts and mixing angles but negligible ones to the n-d ones. (ii) The $T_\alpha = 1/2$ channels with the largest values of $\ell_{12,\alpha}$ (fourth class for $J^\pi = 1/2^+$ and fifth one for $J^\pi = 1/2^-$) give negligible contributions. This implies that $\ell_{12,\alpha} \leqslant 6$ is enough to have accurate results. (iii) The convergence with respect to the grand angular momentum for the first class is the most problematic and it depends noticeably on the interaction. For example, for $J^\pi = 1/2^+$, when the nonlocal potential N3LO-Idaho is used, values of G_1 up to 80 have been found to be necessary (see Table IV). However, in the case of the local AV18, we have verified that within the HH expansion (i.e., without the correlation) $G_1 = 160$ is needed to reach the same degree of accuracy. This is related to the fact that the AV18 potential is more repulsive at short interparticle distances, and therefore the corresponding wave functions in that region are more difficult to be constructed. In fact, when the calculation is performed using the $V_{\text{low-}k}$ potential model, which is very soft at short interparticle distances, it is sufficient to set $G_1 = 40$. A completely identical pattern of convergence is found for all other J^π waves. (iv) The convergence of the other classes is usually faster than for the first class, as it is evident for the cases reported in Tables IV and V. For the $J^\pi = 1/2^+$ case, we obtain convergence with just $G_{2,3,4,5} = 20$. For $J^\pi = 1/2^-$, we have to consider fairly large values of G only for the fourth class (up to $G_4 = 51$), because the channels belonging to this class (the channels 11–14 as reported in Table II) are needed to describe pairs in orbital angular momentum $\ell_2 = 2$. Namely, together with the channels of the first class, they are needed to have a good descriptions of the pairs in the deuteron waves. We have also found that the convergence rate of these classes does not depend much on the nonlocal interaction model. For example, with the $V_{\text{low-}k}$ potential, convergence is achieved with $G_{2,3,4,5} = 20$ for $J^\pi = 1/2^+$ and $G_{2,4} = 31$, $G_{3,5,6} = 21$ for $J^\pi = 1/2^-$. However, note that for the AV18 potential model, we need to set $G_2 = 90$, $G_{3,4,5} = 40$ for $J^\pi = 1/2^+$ and $G_2 = 61$, $G_{3,6} = 41$, $G_4 = 91$, $G_5 = 21$ for $J^\pi = 1/2^-$. A similar pattern of convergence has been found for all the calculated quantities. From now on, all the results which will be presented have been obtained at convergence in the basis expansion.

The results for the n-d and p-d doublet and quartet scattering lengths are given in Table VI and are compared with the available experimental data [26,27]. The results for the AV18 and AV18/UIX have been taken from Ref. [10]. Comparing the theoretical and experimental results for ${}^2a_{nd}$ and ${}^4a_{nd}$, we can conclude that ${}^4a_{nd}$ is very little model-dependent (as well as ${}^4a_{pd}$), and there is a satisfactory agreement between theory and experiment. On the contrary, ${}^2a_{nd}$ is strongly model dependent, and only the inclusion of the TNI brings the theoretical value close to the experimental one. However, some disagreement still remains, and the recent measurement of Ref. [27] is not well described by any of the potential models considered. Though, the N3LO-Idaho/UIXp and N3LO-Idaho/N2LO models give slightly better results. Note that the AV18/UIX results obtained including also MM interaction effects are ${}^2a_{nd} = 0.590$ fm and ${}^4a_{nd} = 6.343$ fm. Finally, the $V_{\text{low-}k}$ results are in remarkable disagreement with the experimental data, and a sizable difference from the AV18/UIX results is also observed. Therefore, even when the cutoff parameter of the $V_{\text{low-}k}$ interaction model is fixed to reproduce the triton binding energy, the doublet scattering length is not well reproduced. This observation seems to suggest that the S-wave sensitive scattering observables, like the scattering lengths, are not properly described by simply increasing the attraction, but a right balance between attraction and repulsion of the nuclear force has to be reached. Such a balance cannot be achieved with just one parameter, as the cutoff Λ of the $V_{\text{low-}k}$ interaction. Further analysis of these aspects is currently underway [28].

The p-d elastic-scattering observables have been studied at different values of center-of-mass energy $E_{\text{c.m.}}$. Because we have considered several interaction models, we first focus our attention on the two-nucleon only models, i.e., the AV18 and the N3LO-Idaho. The differential cross section $d\sigma/d\Omega$, the proton vector analyzing power A_y, and the deuteron vector and tensor analyzing powers iT_{11}, T_{20}, T_{21}, and T_{22}, as function of the center-of-mass angle $\theta_{\text{c.m.}}$, are given in Figs. 1–6, respectively. The data are taken from Refs. [29–35], as indicated in detail in the figure captions. By inspection of

TABLE VI. n-d and p-d doublet and quartet scattering lengths in fm calculated with the HH technique using different Hamiltonian models.

Interaction	${}^2a_{nd}$	${}^4a_{nd}$	${}^2a_{pd}$	${}^4a_{pd}$
AV18	1.275	6.325	1.185	13.588
AV18/UIX	0.610	6.323	−0.035	13.588
N3LO-Idaho	1.099	6.342	0.876	13.646
N3LO-Idaho/UIXp	0.623	6.343	−0.007	13.647
N3LO-Idaho/N2LO	0.675	6.342	0.072	13.647
$V_{\text{low-}k}$	0.572	6.321	−0.001	13.571
Exp. [26]	0.65 ± 0.04	6.35 ± 0.02		
Exp. [27]	$0.645 \pm 0.003 \pm 0.007$	–		

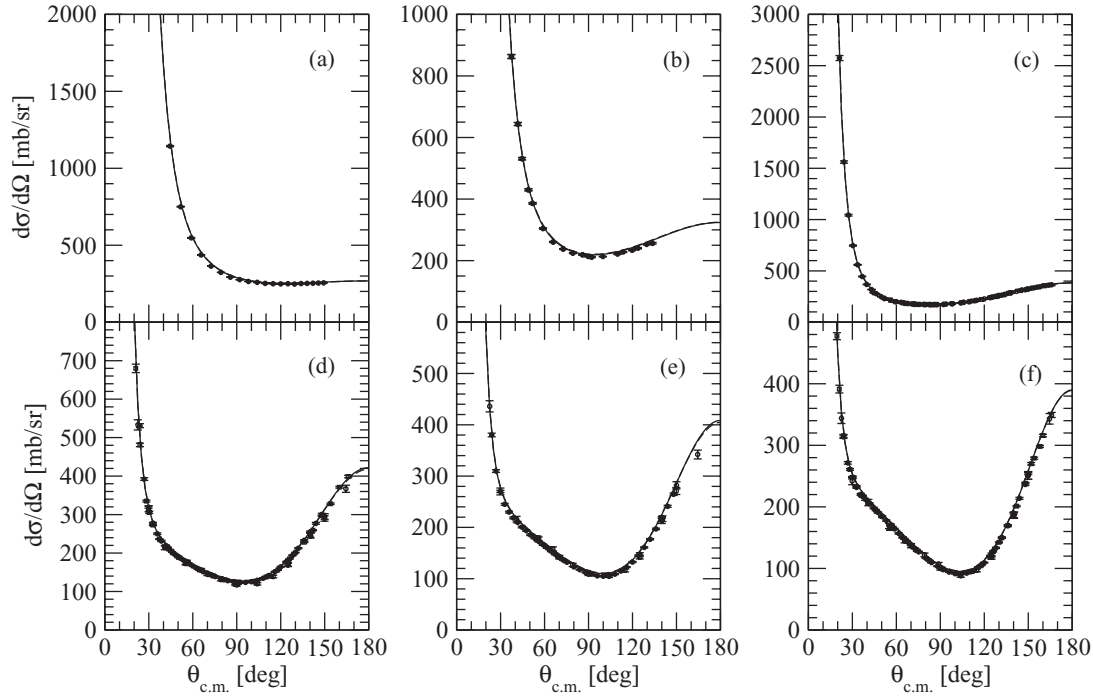

FIG. 1. *p-d* differential cross section calculated with the AV18 (dashed lines) and the N3LO-Idaho (solid lines) two-nucleon potential models. Panels (a)–(f) correspond to center-of-mass energies $E_{\text{c.m.}} = 0.266, 0.431, 0.666, 1.33, 1.66,$ and 2.0 MeV, respectively. Data are from Ref. [29] at $E_{\text{c.m.}} = 0.266$ MeV; from Ref. [30] at $E_{\text{c.m.}} = 0.431$ MeV; from Refs. [29] (solid circles), [31] (empty circles), and [32] (empty squares) at $E_{\text{c.m.}} = 0.666$ MeV; from Refs. [32] (empty squares: $E_p = 1.993$ MeV), [33] (solid circles), and [34] (empty circles: $E_p = 2.08$ MeV) at $E_{\text{c.m.}} = 1.33$ MeV; from Refs. [33] (solid circles) and [34] (empty circles: $E_p = 2.53$ MeV) at $E_{\text{c.m.}} = 1.66$ MeV; and from Refs. [33] (solid circles), [32] (empty squares: $E_p = 2.995$ MeV), and [34] (empty circles) at $E_{\text{c.m.}} =$ 2.0 MeV.

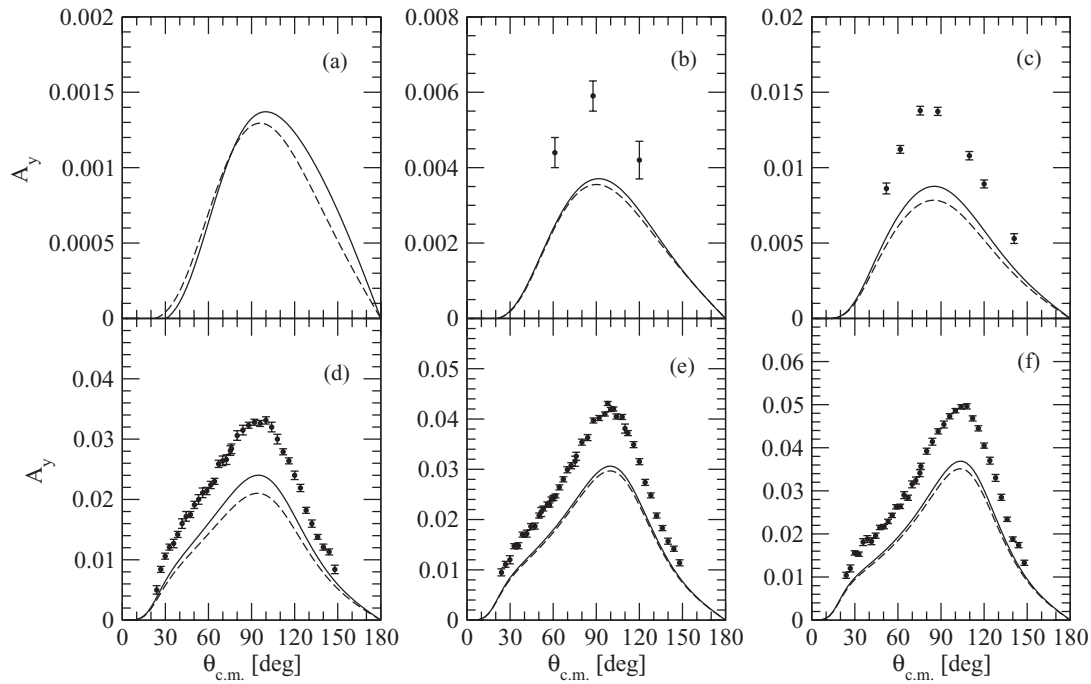

FIG. 2. Same as in Fig. 1 but for the proton vector analyzing power A_y. Data are from Ref. [30] at $E_{\text{c.m.}} = 0.431$ MeV, from Ref. [35] at $E_{\text{c.m.}} = 0.666$ MeV, and from Ref. [33] at $E_{\text{c.m.}} = 1.33, 1.66,$ and 2.0 MeV.

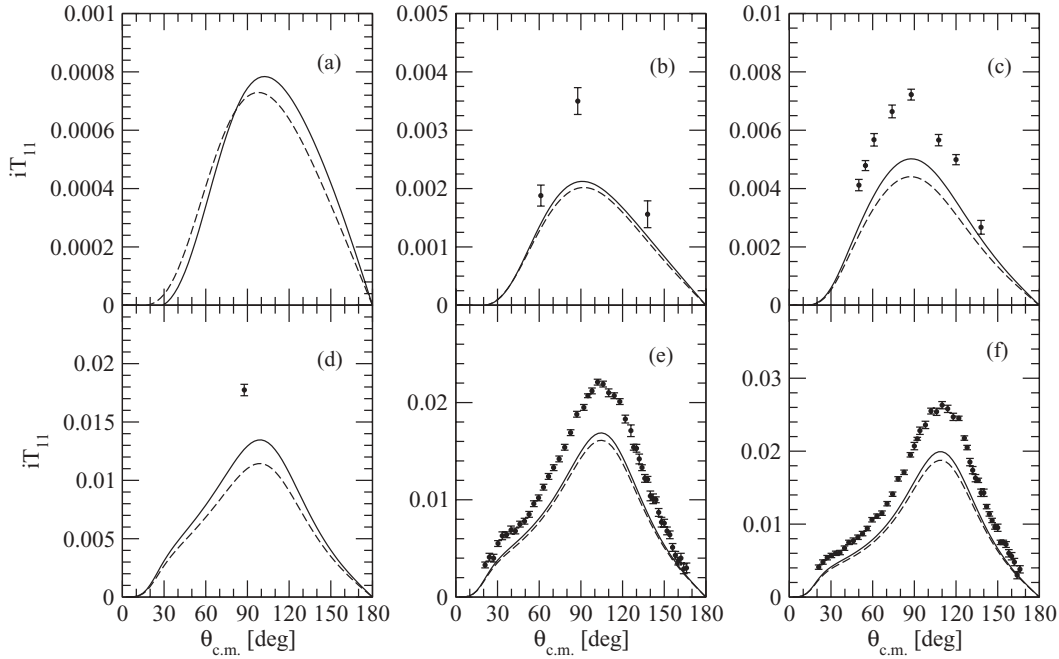

FIG. 3. Same as in Fig. 1 but for the deuteron vector analyzing power iT_{11}. Data are from Ref. [30] at $E_{\text{c.m.}} = 0.431$ and 1.33 MeV, from Ref. [35] at $E_{\text{c.m.}} = 0.666$ MeV, and from Ref. [33] at $E_{\text{c.m.}} = 1.66$ and 2.0 MeV.

the figures, we can observe that (i) theory and experiment are in disagreement for the A_y and iT_{11} observables (the well-known "A_y-puzzle" [24,36]); (ii) no differences between the AV18 and the N3LO-Idaho curves can be seen for the differential cross sections; (iii) the N3LO-Idaho curves are systematically closer to the data than the AV18 ones for the polarization observables, especially for A_y and iT_{11}. The reason of this behavior is well known [16] and is related to the MM interaction. In fact, the AV18 potential model has been constructed keeping the electromagnetic interaction separated

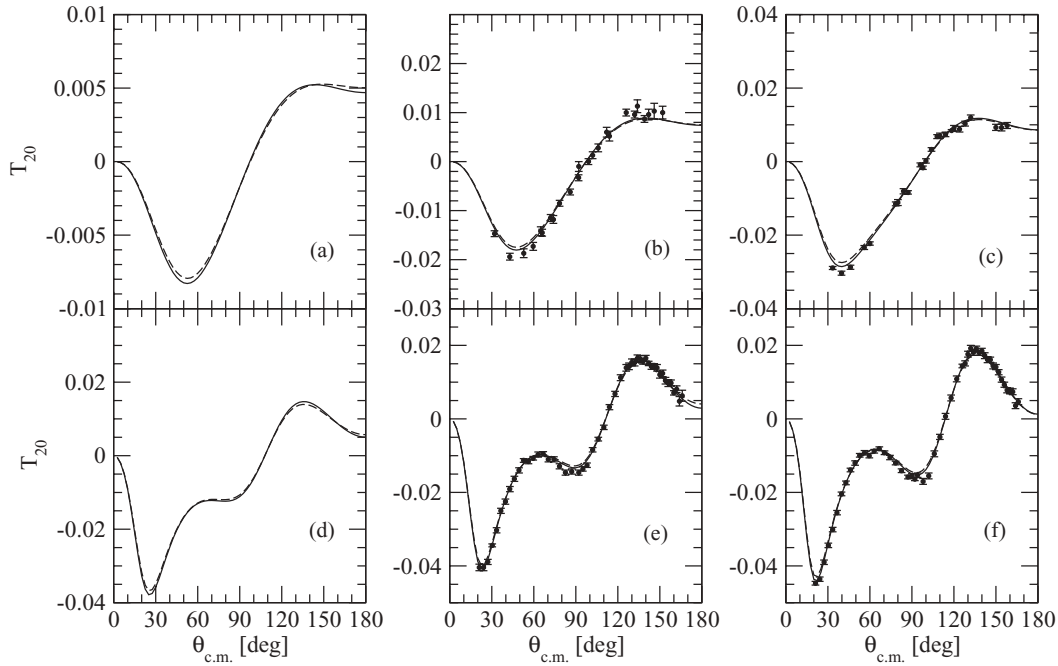

FIG. 4. Same as in Fig. 1 but for the deuteron tensor analyzing power T_{20}. Data are from Ref. [30] at $E_{\text{c.m.}} = 0.431$ MeV, from Ref. [35] at $E_{\text{c.m.}} = 0.666$ MeV, and from Ref. [33] at $E_{\text{c.m.}} = 1.66$ and 2.0 MeV.

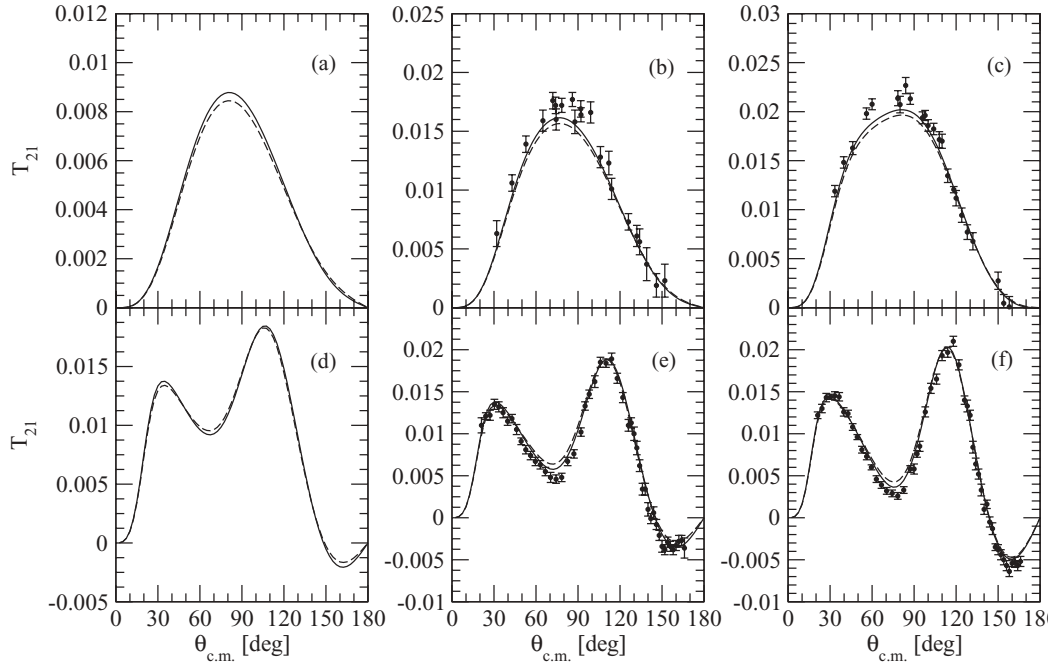

FIG. 5. Same as in Fig. 1 but for the deuteron tensor analyzing power T_{21}. Data are from the same references as in Fig. 4.

from the nuclear one. The electromagnetic interaction includes the MM one, as well as higher-order corrections to the *pp* Coulomb potential as two-photon exchange, Darwin-Foldy, and vacuum polarization terms. The MM interaction effects are known to be sizable in *N-d* elastic scattering [16]. On the contrary, the N3LO-Idaho potential model keeps as electromagnetic interaction only the point Coulomb potential and MM effects are indirectly included in the nuclear part of the interaction by the fitting procedure. From this observation, we can guess that the results obtained with the two-nucleon potentials AV18 and N3LO-Idaho should be comparable when the AV18 calculation includes also the MM effects. To verify this hypothesis, we have calculated the *p-d* elastic-scattering observables at two values of $E_{\text{c.m.}}$, 1.33 and 2.0 MeV, using

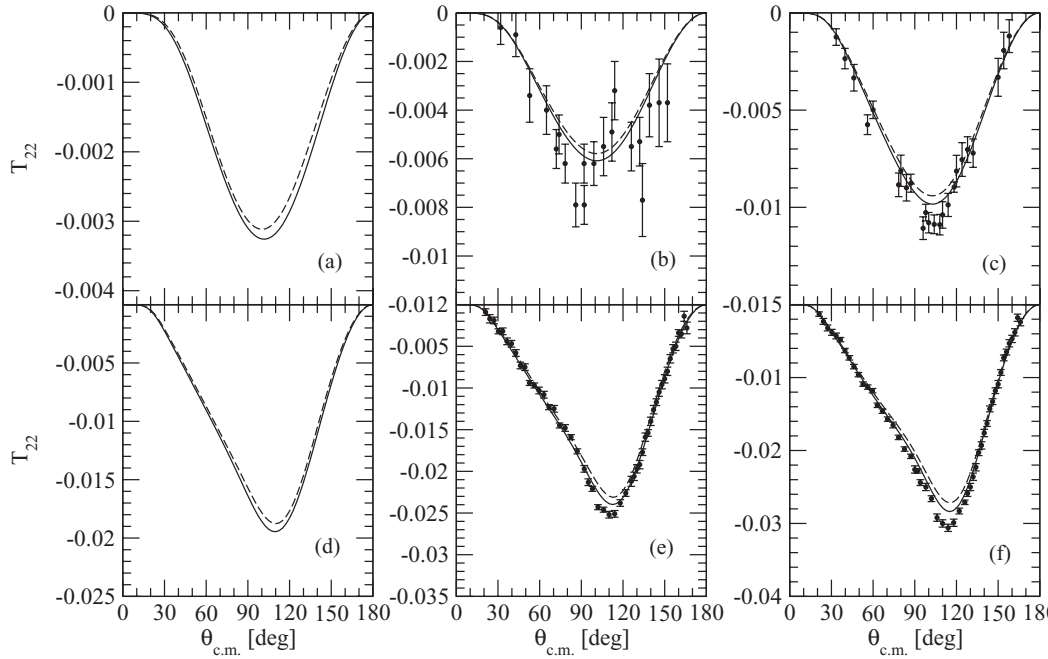

FIG. 6. Same as in Fig. 1 but for the deuteron tensor analyzing power T_{22}. Data are from the same references as in Fig. 4.

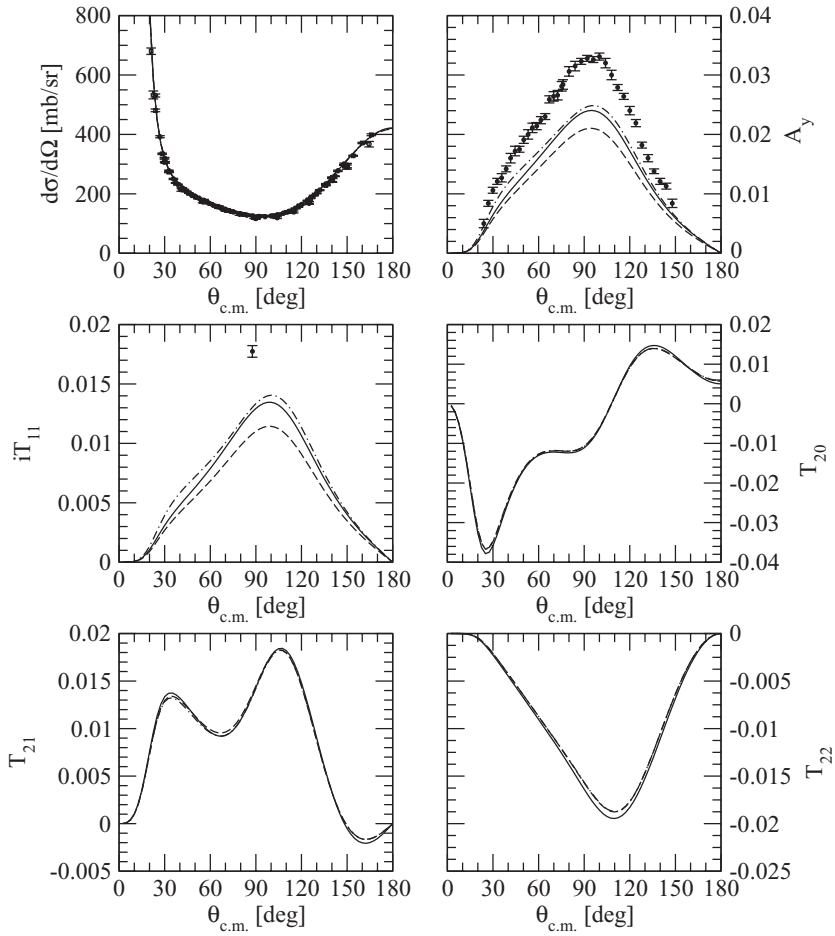

FIG. 7. Theoretical results for p-d differential cross section $d\sigma/d\Omega$, and polarization observables A_y, iT_{11}, T_{20}, T_{21}, and T_{22}, at $E_{\text{c.m.}} = 1.33$ MeV are compared to the experimental data. The calculation are done using the AV18 (dashed lines), the AV18 + MM (dotted-dashed lines), and the N3LO-Idaho (solid lines) interactions. The data are from Refs. [32] (empty squares: $E_p = 1.993$ MeV), [33] (solid circles), and [34] (empty circles: $E_p = 2.08$ MeV) for the differential cross section and from Refs. [33] and [30] for the A_y and iT_{11} polarization observables, respectively. The incident proton (deuteron) is $E_p = 2.0$ MeV ($E_d = 4.0$ MeV).

the AV18, AV18 + MM, and N3LO-Idaho potential models. The results are given in Figs. 7 and 8, respectively. From inspection of the figures, we can notice that the AV18 + MM results for the A_y and iT_{11} vector polarization observables are larger than the AV18 alone ones in the maximum region and that the AV18 + MM and N3LO-Idaho curves are quite close to each other for all the observables considered. Although this analysis should be performed systematically at any value of $E_{\text{c.m.}}$ and for any observable, given the conclusions of Ref. [16], it can be expected that a similar behavior still holds. Therefore, we can conclude that the nonlocal N3LO-Idaho and the local AV18 two-nucleon interactions give similar results once the MM effects are included in the AV18 calculation. For this reason, we have chosen to use the N3LO-Idaho two-nucleon interaction model in the continuation of our study.

To have a meaningful comparison with the data, the TNI cannot be neglected in the calculation. Therefore, we present in Figs. 9–14 the results for the different observables, obtained with the N3LO-Idaho two-nucleon interaction models and the N3LO-Idaho/UIXp and N3LO-Idaho/N2LO two- and three-nucleon interaction models. From inspection of the figures, we can observe that the TNI effects are sizable, especially for the polarization observables, and the N3LO-Idaho/N2LO

TABLE VII. χ^2/datum of the p-d elastic-scattering observables at $E_{\text{c.m.}} = 0.666$, 1.33, 1.66, and 2.0 MeV, calculated with the N3LO-Idaho two-nucleon only, and the N3LO-Idaho/UIXp and N3LO-Idaho/N2LO two- plus three-nucleon Hamiltonian models. The different number N of experimental data is also indicated. The data are from Refs. [31,35] at $E_{\text{c.m.}} = 0.666$ MeV and from Ref. [33] at $E_{\text{c.m.}} = 1.33$, 1.66, and 2.0 MeV.

	0.666 MeV					1.33 MeV	1.66 MeV					2.0 MeV				
	A_y	iT_{11}	T_{20}	T_{21}	T_{22}	A_y	A_y	iT_{11}	T_{20}	T_{21}	T_{22}	A_y	iT_{11}	T_{20}	T_{21}	T_{22}
N	7	8	24	24	24	38	44	50	50	50	50	38	51	51	51	51
N3LO-Idaho	197.7	68.7	4.0	2.6	1.5	108.4	227.9	92.6	1.0	2.2	2.7	186.0	108.3	1.9	2.8	4.4
N3LO-Idaho/UIXp	171.2	53.1	2.6	2.2	0.9	89.2	185.9	67.0	2.0	3.2	3.2	152.5	81.8	3.0	5.5	1.6
N3LO-Idaho/N2LO	139.9	49.5	2.7	2.5	0.9	70.0	159.4	84.3	2.1	4.0	2.8	114.0	85.8	3.6	8.3	1.6

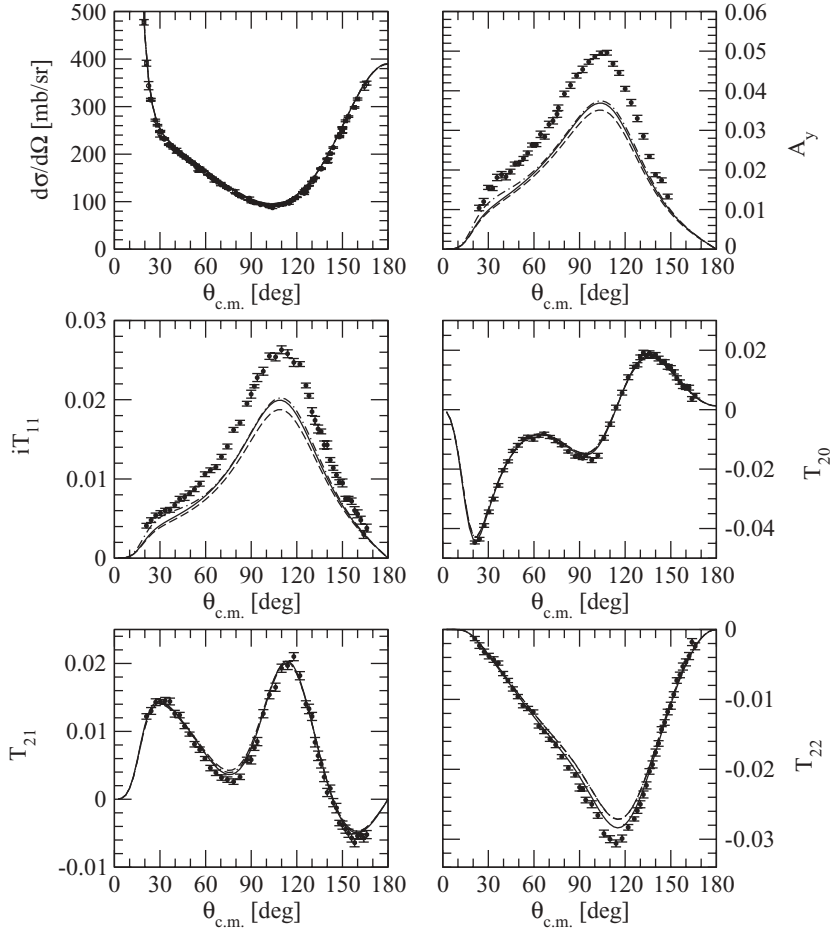

FIG. 8. Same as in Fig. 7 but for $E_{\mathrm{c.m.}} = 2.0$ MeV. The data are from Refs. [33] (solid circles), [32] (empty squares: $E_p = 2.995$ MeV), and [34] (empty circles) for the differential cross section, and from Ref. [33] for the polarization observables. The incident proton (deuteron) is $E_p = 3.0$ MeV ($E_d = 6.0$ MeV).

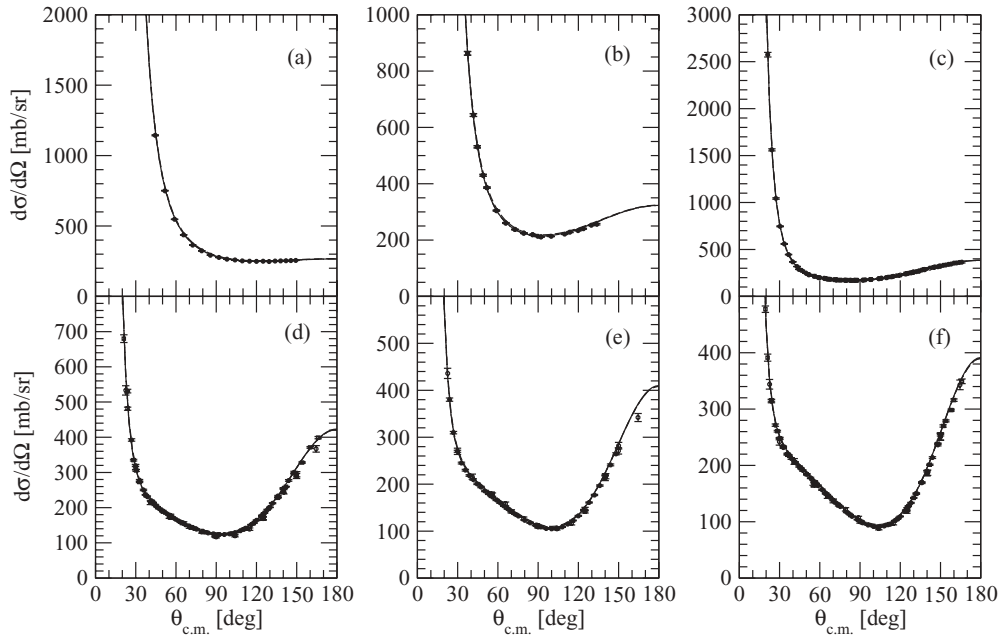

FIG. 9. *p-d* differential cross section calculated with the N3LO-Idaho (dashed lines), the N3LO-Idaho/UIXp (dotted-dashed lines), and the N3LO-Idaho/N2LO (solid lines) two- and three-nucleon interaction models. Panels (a)–(f) correspond to center-of-mass energies $E_{\mathrm{c.m.}} = 0.266$, 0.431, 0.666, 1.33, 1.66, and 2.0 MeV, respectively. Data are from the same references as in Fig. 1.

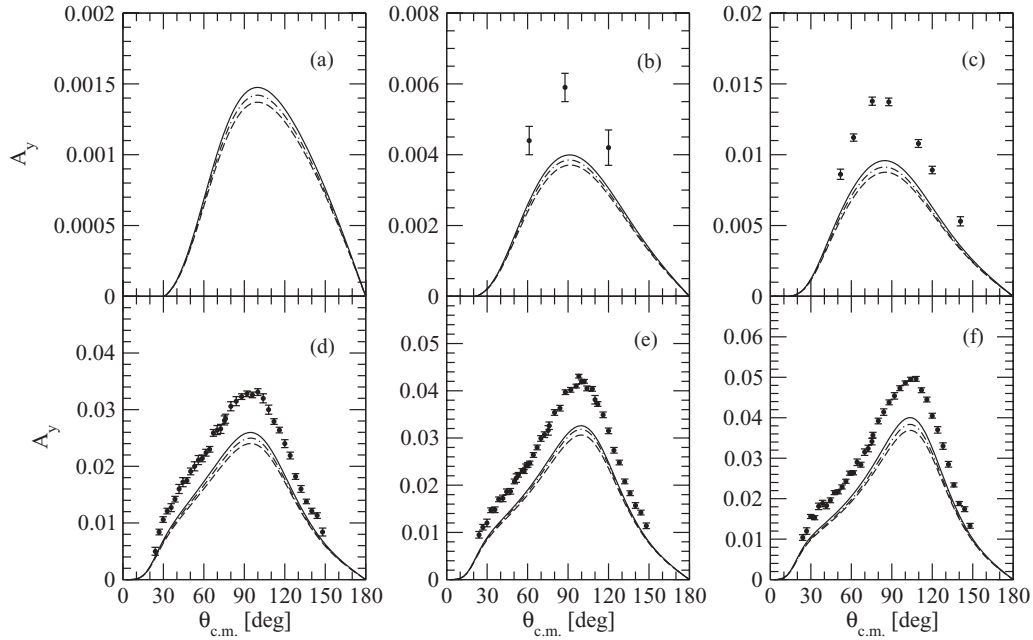

FIG. 10. Same as in Fig. 9, but for the proton vector analyzing power A_y. Data are from the same references as in Fig. 2.

potential model gives a slightly better description of the data than the N3LO-Idaho/UIXp one. In particular, it is interesting to note that the A_y and iT_{11} observables are better described at every value of $E_{\text{c.m.}}$, except for iT_{11} at $E_{\text{c.m.}} = 1.66$ MeV, although even in this case all the curves are very close to each other.

For a better comparison between the different potential models and the data, a χ^2 analysis has been carried only for those observables, except the differential cross section, for which the number of data N is $N \geqslant 7$. In particular, following Ref. [31],

$$\chi^2/\text{datum} = \frac{1}{N}\sum_i \frac{\left(f_i^{\text{exp}} - f_i^{\text{th}}\right)^2}{(\Delta f_i)^2} \tag{3.1}$$

where f_i^{exp} is the ith datum at center-of-mass angle θ_i, Δf_i is its experimental error, and f_i^{th} is the theoretical value at the same angle. The results are given in Table VII for

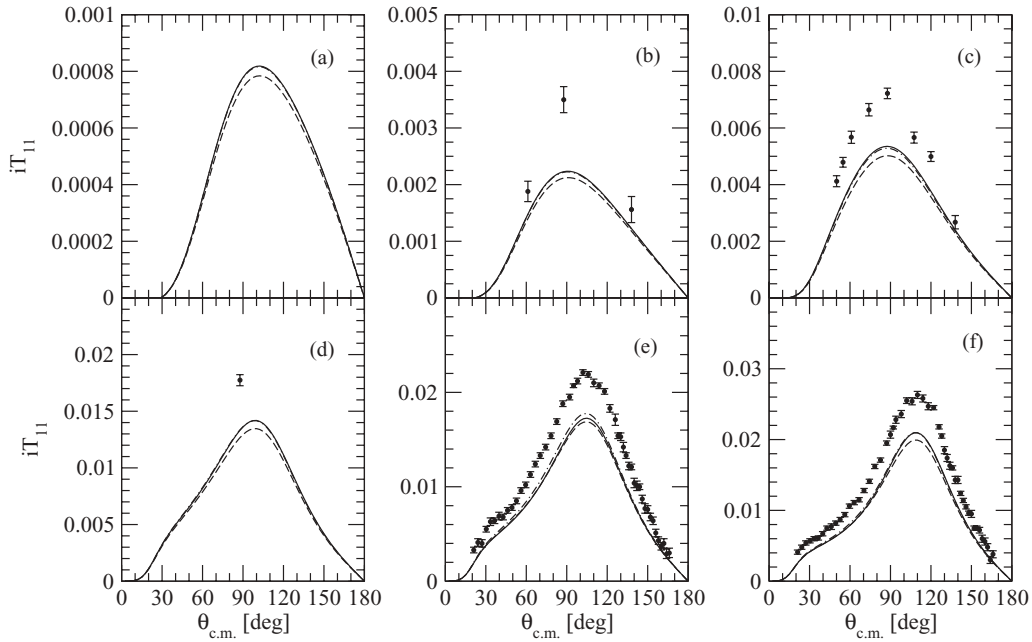

FIG. 11. Same as in Fig. 9, but for the deuteron vector analyzing power iT_{11}. Data are from the same references as in Fig. 3.

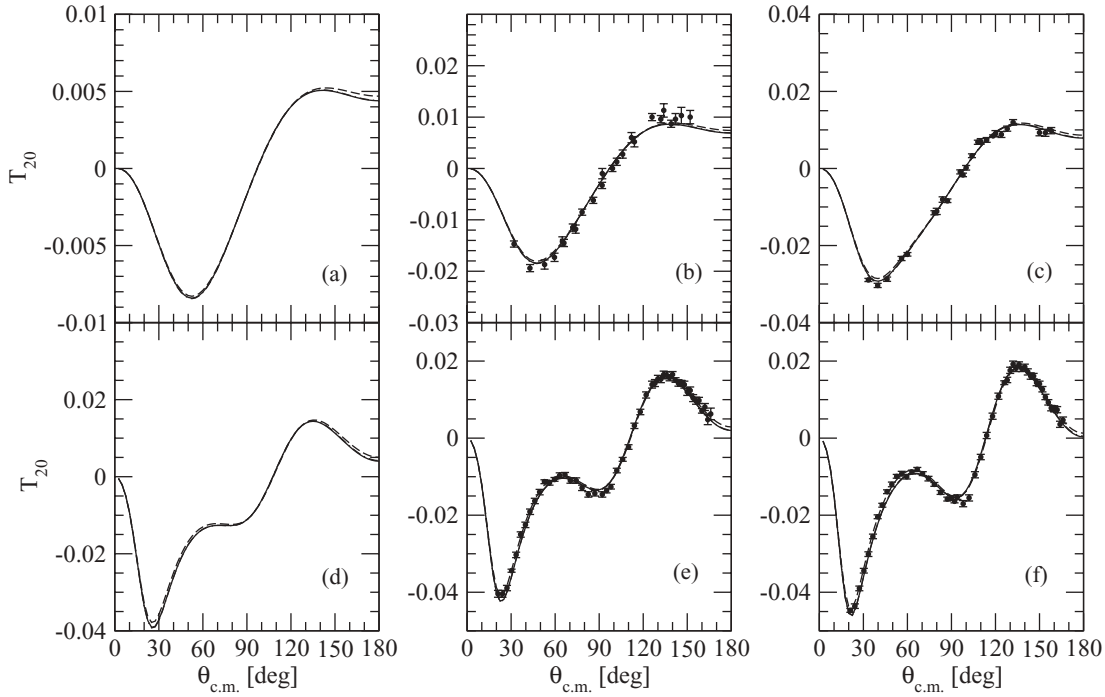

FIG. 12. Same as in Fig. 9 but for the deuteron tensor analyzing power T_{20}. Data are from the same references as in Fig. 4.

$E_{\text{c.m.}} = 0.666$, 1.33, 1.66, and 2.0 MeV. The N3LO-Idaho, N3LO-Idaho/UIXp, and N3LO-Idaho/N2LO interaction models have been considered. From inspection of the table we can note that all the values for χ^2/datum are comparable, although the ones obtained with the N3LO-Idaho two-nucleon interaction are usually higher than the ones obtained with two- and three-nucleon interactions, except for the tensor analyzing power T_{20} and T_{21}. This is a well-known and still unclear

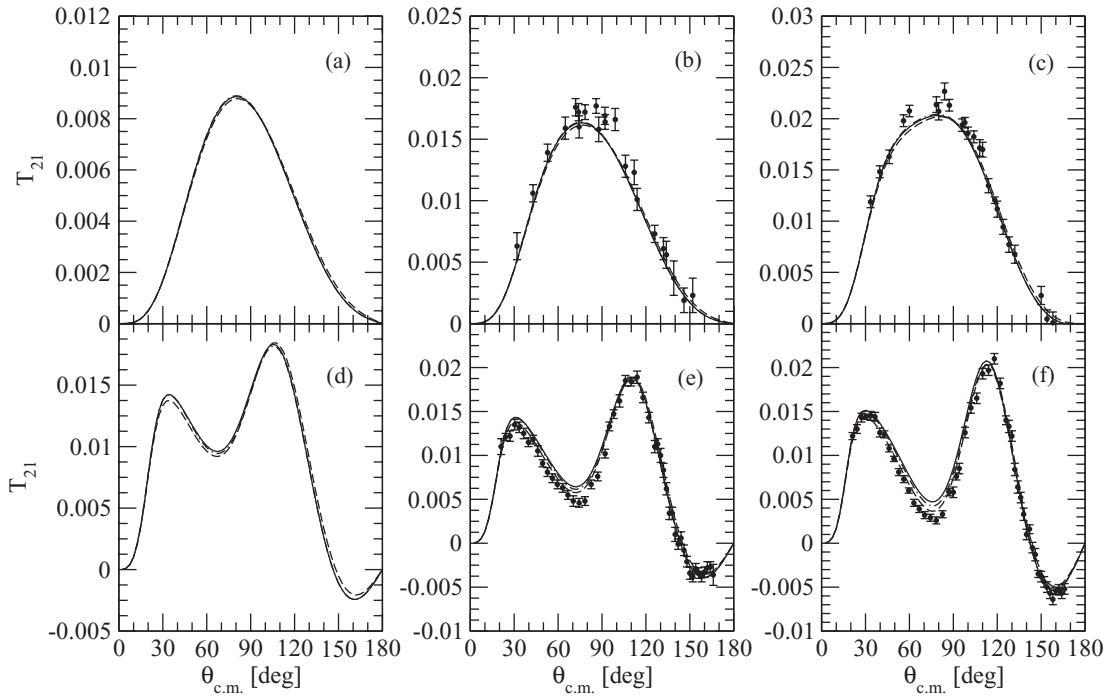

FIG. 13. Same as in Fig. 9 but for the deuteron tensor analyzing power T_{21}. Data are from the same references as in Fig. 5.

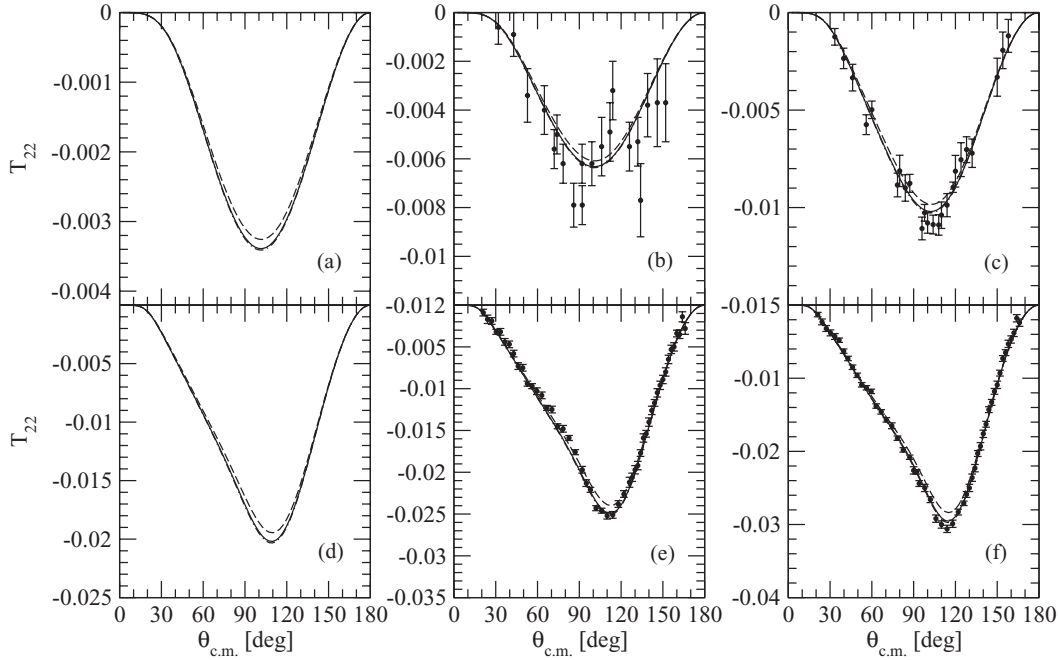

FIG. 14. Same as in Fig. 9 but for the deuteron tensor analyzing power T_{22}. Data are from the same references as in Fig. 6.

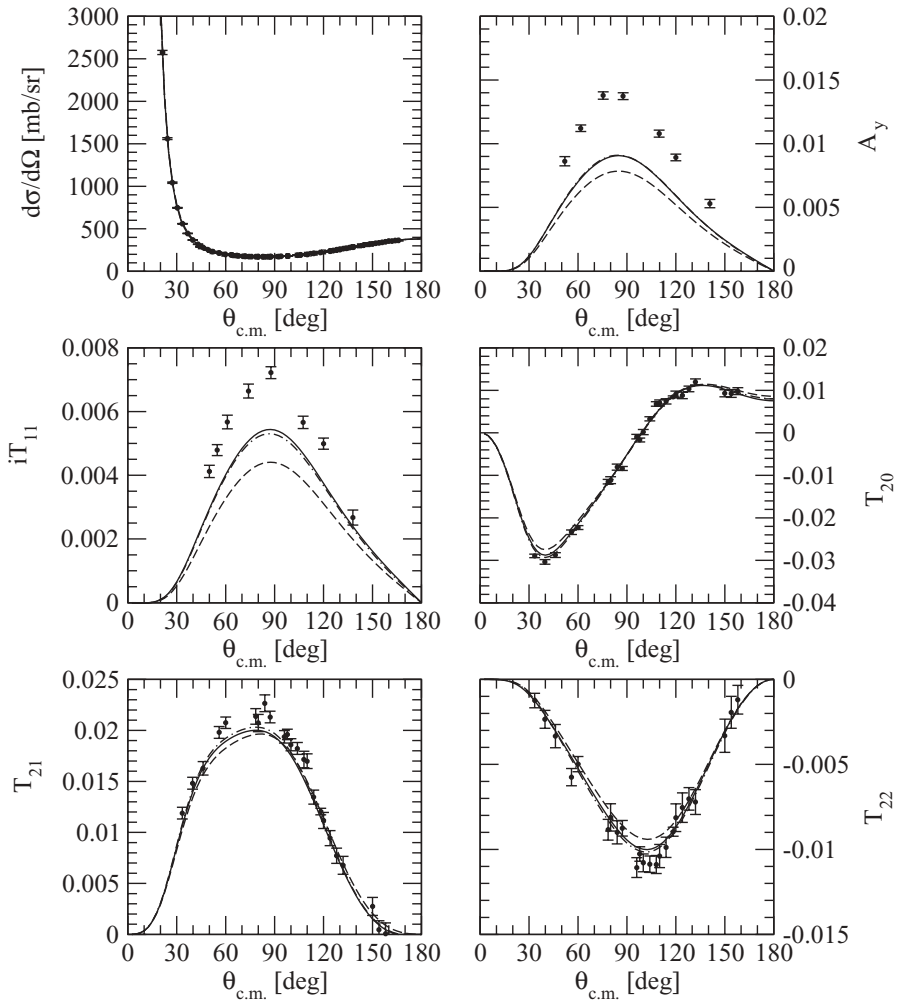

FIG. 15. The theoretical values of the p-d differential cross section $d\sigma/d\Omega$, A_y, iT_{11}, T_{20}, T_{21}, and T_{22}, at $E_{\text{c.m.}} = 0.666$ MeV are compared to the experimental data. The calculations are done with the AV18 (dashed lines), the AV18/UIX (dotted-dashed lines), and the $V_{\text{low-}k}$ two-nucleon interaction, obtained from the AV18 with a cutoff parameter $\Lambda = 2.2$ fm^{-1} (solid lines). The data are from Refs. [29] (solid circles), [31] (empty circles), and [32] (empty squares) for the differential cross section and from Ref. [35] for the polarization observables. The incident proton (deuteron) is $E_p = 1.0$ MeV ($E_d = 2.0$ MeV).

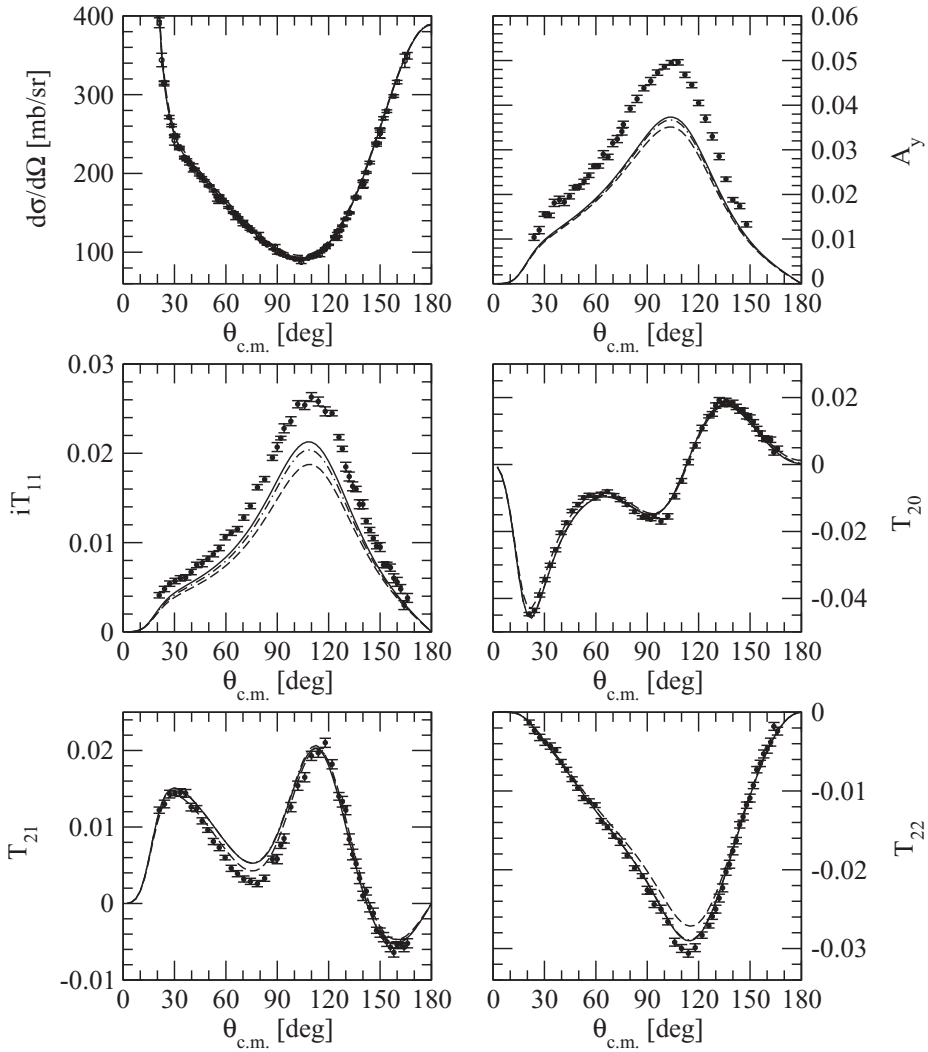

FIG. 16. Same as in Fig. 15 but at $E_{\text{c.m.}} = 2.0$ MeV. The data are from Refs. [33] (solid circles), [32] (empty circles), and [34] (empty squares) for the differential cross section and from Ref. [33] for the polarization observables. The incident proton (deuteron) is $E_p = 3.0$ MeV ($E_d = 6.0$ MeV).

issue, i.e., T_{20} and T_{21} are better described, as the energy increases, by two-nucleon only interaction models, even at 30.0 MeV [37]. Among the two- plus three-nucleon interaction models, the N3LO-Idaho/N2LO performs slightly better than the N3LO-Idaho/UIXp.

The *p-d* elastic-scattering observables at $E_{\text{c.m.}} = 0.666$ and 2.0 MeV have been calculated also using the two-nucleon only potential model $V_{\text{low-}k}$, obtained from the AV18 with a cutoff parameter Λ equal to 2.2 fm^{-1}, as already used for the calculation of the scattering lengths. The results are given in Figs. 15 and 16, respectively. Together with the $V_{\text{low-}k}$ results, we have shown also the bare AV18 and the AV18/UIX ones. From inspection of the figures, we can observe that the $V_{\text{low-}k}$ results are very similar to the AV18/UIX ones. This can be understood noticing that the considered observables are sensitive to *P*- and *D*-wave scattering. The *P*-wave phase shifts and mixing angles are influenced by the UIX TNI attraction term, which is reproduced, within the $V_{\text{low-}k}$ approach, by fitting the cutoff parameter Λ. In fact, the $J^\pi = 1/2^-$ phase shifts and mixing angle ($\delta_{1\frac{1}{2}\frac{1}{2}}, \delta_{1\frac{3}{2}\frac{1}{2}}, \epsilon_{\frac{1}{2}^-}$) obtained at $E_{\text{c.m.}} = 2.0$ MeV with the AV18, AV18/UIX, and $V_{\text{low-}k}$ potential models are $(-7.358, 22.11, 5.718)$, $(-7.366, 22.32, 5.835)$, and $(-7.343, 22.26, 5.811)$, respectively. From this first analysis of $V_{\text{low-}k}$ results for *N-d* scattering at low energies, we can conclude that the $V_{\text{low-}k}$ and AV18/UIX results are close to each other for observables sensitive to *P*- and *D*-wave scattering, like vector and tensor analyzing powers. Further work on these aspects is currently underway.

The *n-d* elastic-scattering observables, including differential cross section, neutron vector analyzing power A_y, deuteron vector and tensor analyzing powers iT_{11}, T_{20}, T_{21}, and T_{22}, at $E_{\text{c.m.}} = 1.33$ and 2.0 MeV are given in Figs. 17 and 18, respectively. The experimental data are from Refs. [38–40] and Refs. [41,42] at $E_{\text{c.m.}} = 1.33$ MeV and 2.0 MeV, respectively. The different curves are obtained using the N3LO-Idaho, N3LO-Idaho/UIXp, and N3LO-Idaho/N2LO potential models. From inspection of the figures, we can observe that all the curves are very close to each other, especially for the differential cross section $d\sigma/d\Omega$ and the tensor analyzing powers T_{20}, T_{21}, and T_{22}, although some small differences are appreciable. Moreover, some differences are

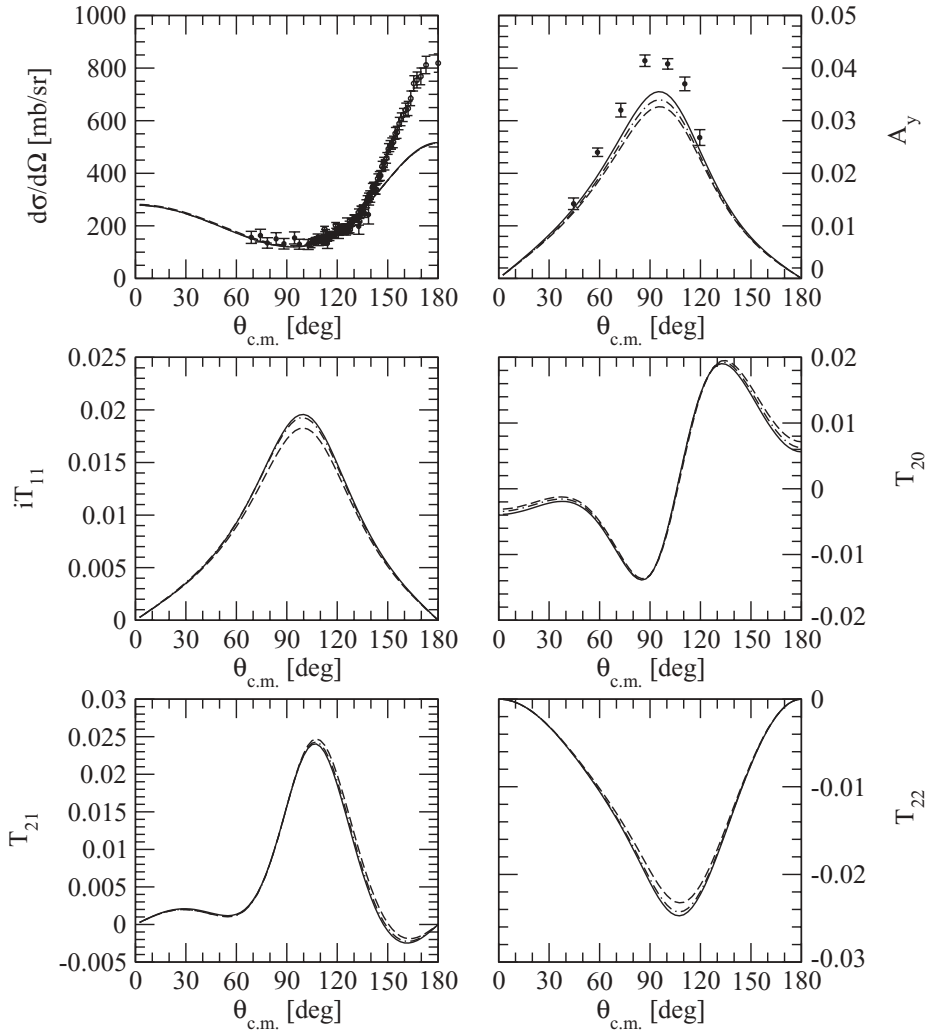

FIG. 17. n-d differential cross section $d\sigma/d\Omega$, A_y, iT_{11}, T_{20}, T_{21}, and T_{22}, at $E_{\text{c.m.}} = 1.33$ MeV are calculated with the N3LO-Idaho (dashed line), the N3LO-Idaho/UIXp (dotted-dashed line), and the N3LO-Idaho/N2LO (solid line) potential models. The experimental data are of Refs. [38] (solid circles) and [39] (empty squares: $E_n = 2.016$ MeV) for $d\sigma/d\Omega$ and Ref. [40] for A_y. The incident neutron (deuteron) is $E_n = 2.0$ MeV ($E_d = 4.0$ MeV).

present for the A_y and iT_{11} vector polarization observables at the peak, even if TNI effects are small. Comparing the calculations with the data, we can observe that the calculated $d\sigma/d\Omega$ at $E_{\text{c.m.}} = 1.33$ MeV is much lower than the measured one for large values of the center-of-mass angle $\theta_{\text{c.m.}}$. Such a discrepancy, however, disappears at $E_{\text{c.m.}} = 2.0$ MeV. This difference has been observed before and its origin has still to be clarified [23]. As in the p-d case, the n-d vector analyzing powers A_y are poorly described by the theory in the maximum region, but it should be noted that the N3LO-Idaho/N2LO gives again a better description of the observables than the N3LO-Idaho/UIXp Hamiltonian model.

IV. CONCLUSIONS

Following our previous studies on the HH method revisited to work in momentum space [10,15], we have implemented our technique to study the N-d elastic-scattering problem at center-of-mass energies below deuteron breakup threshold, using both local and nonlocal realistic nuclear interactions. Using this method, it is possible to accurately calculate N-d scattering observables at very low energies, including the contribution from the Coulomb potential as well as from higher-order electromagnetic terms, such as the MM interaction. In particular, it is the first time that nuclear model including nonlocal two-nucleon interactions plus TNIs are used to describe p-d scattering at very low energies. We have studied several observables, as scattering lengths, differential cross section, and vector and tensor analyzing powers, and we have compared our results with the available experimental data. Our main conclusions can be summarized as follows: (i) the results obtained from the local AV18 and the nonlocal N3LO-Idaho two-nucleon interaction differ substantially from each other, especially for the vector polarization observables A_y and iT_{11} in the maximum region. (ii) The differences between AV18 and N3LO-Idaho results are strongly reduced when the MM effects are included in the AV18 calculation. To be noticed that the MM effects are indirectly included in the nuclear N3LO-Idaho interaction, because in the fitting procedure for this model only the point Coulomb interaction between pp is used. (iii) Among the TNIs here considered, the N2LO model performs slightly better than the UIX

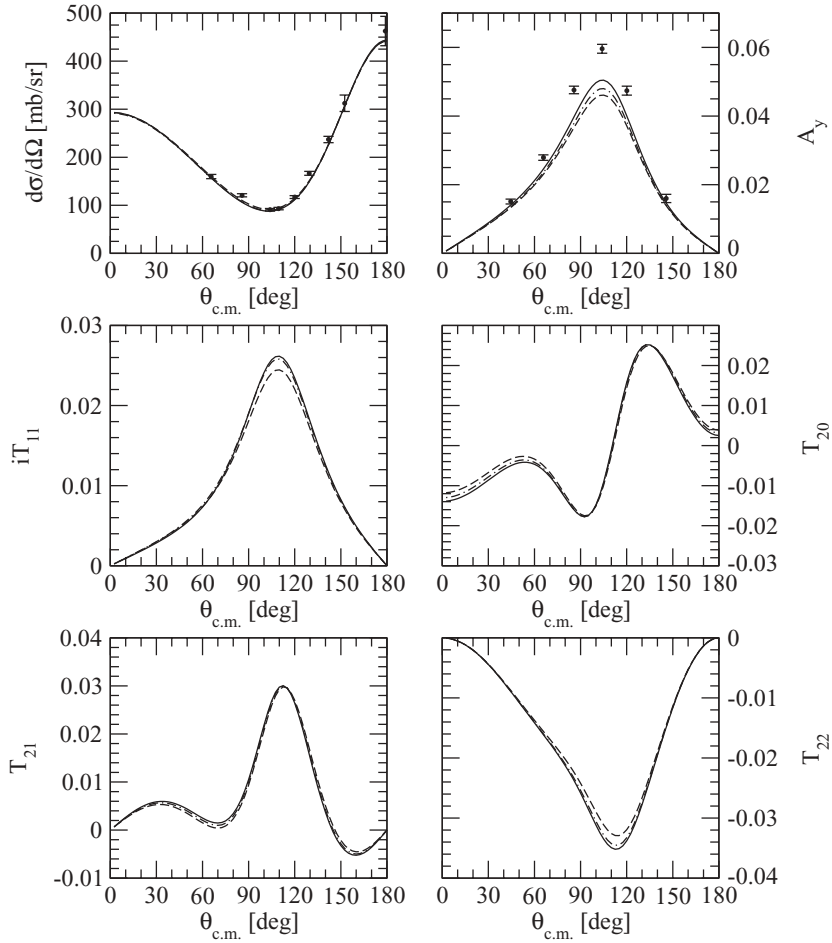

FIG. 18. Same as in Fig. 17 but for $E_{\text{c.m.}} = 2.0$ MeV. The experimental data are from Ref. [41] for $d\sigma/d\Omega$ and Ref. [42] for A_y. The incident neutron (deuteron) is $E_n = 3.0$ MeV ($E_d = 6.0$ MeV).

one. The N3LO-Idaho/N2LO results are in fact generally closer to the experimental data than the N3LO-Idaho/UIXp ones. (iv) The $V_{\text{low-}k}$ two-nucleon interaction model has also been considered, obtained from AV18 with a cutoff parameter $\Lambda = 2.2$ fm^{-1}, fitted to reproduce the triton binding energy. The $V_{\text{low-}k}$ results for those observables sensitive to S-wave scattering, such as the scattering lengths, are in strong disagreement with the experimental data and quite different from the corresponding AV18/UIX ones. On the contrary, the results for those observables sensitive to P- and D-wave scattering, such as vector and tensor analyzing powers, are very similar to the corresponding AV18/UIX ones. Further studies on these aspects are currently underway. We expect to extend the present approach to the $A = 4$ scattering problem below breakup threshold, as already done for zero-energy scattering in Ref. [10].

[1] R. B. Wiringa, V. G. J. Stoks, and R. Schiavilla, Phys. Rev. C **51**, 38 (1995).
[2] R. Machleidt, Phys. Rev. C **63**, 024001 (2001).
[3] E. Epelbaum, W. Glöckle, and Ulf-G. Meissner, Nucl. Phys. **A747**, 362 (2005).
[4] D. R. Entem and R. Machleidt, Phys. Rev. C **68**, 041001(R) (2003).
[5] B. S. Pudliner, V. R. Pandharipande, J. Carlson, and R. B. Wiringa, Phys. Rev. Lett. **74**, 4396 (1995).
[6] E. Epelbaum, A. Nogga, W. Glöckle, H. Kamada, Ulf-G. Meissner, and H. Witala, Phys. Rev. C **66**, 064001 (2002).
[7] P. Navrátil, Few-Body Syst. **41**, 117 (2007).
[8] S. K. Bogner *et al.*, Nucl. Phys. **A784**, 79 (2007).
[9] See, for example, W. Glöckle *et al.*, Phys. Rep. **274**, 107 (1996); J. Carlson and R. Schiavilla, Rev. Mod. Phys. **70**, 743 (1998); H. Witala *et al.*, Phys. Rev. C **73**, 044004 (2006); A. Deltuva, A. C. Fonseca, and S. K. Bogner, *ibid.* **77**, 024002 (2008); P. Doleschall, *ibid.* **77**, 034002 (2008).
[10] A. Kievsky *et al.*, J. Phys. G: Nucl. Part. Phys. **35**, 063101 (2008).
[11] A. Kievsky, M. Viviani, and S. Rosati, Nucl. Phys. **A551**, 241 (1993).
[12] A. Kievsky, M. Viviani, and S. Rosati, Nucl. Phys. **A577**, 511 (1994).
[13] A. Kievsky *et al.*, Few-Body Syst. **22**, 1 (1997).
[14] M. Viviani, A. Kievsky, and S. Rosati, Phys. Rev. C **71**, 024006 (2005).
[15] M. Viviani *et al.*, Few-Body Syst. **39**, 159 (2006).
[16] A. Kievsky, M. Viviani, and L. E. Marcucci, Phys. Rev. C **69**, 014002 (2004).
[17] M. Fabre de la Ripelle, Ann. Phys. **147**, 281 (1983).
[18] J. Raynal and J. Revai, Il Nuovo Cim. **68**, 612 (1970).

[19] C. R. Chen, G. L. Payne, J. L. Friar, and B. F. Gibson, Phys. Rev. C **39**, 1261 (1989).
[20] W. Kohn, Phys. Rev. **74**, 1763 (1948).
[21] A. Kievsky, Nucl. Phys. **A624**, 125 (1997).
[22] L. E. Marcucci *et al.*, Few-Body Syst. **44**, 207 (2008).
[23] A. Kievsky *et al.*, Nucl. Phys. **A607**, 402 (1996).
[24] A. Kievsky, M. Viviani, and S. Rosati, Phys. Rev. C **52**, R15 (1995).
[25] H. Kameyama, M. Kamimura, and Y. Fukushima, Phys. Rev. C **40**, 974 (1989).
[26] W. Dilg *et al.*, Phys. Lett. **B36**, 208 (1971).
[27] K. Schoen *et al.*, Phys. Rev. C **67**, 044005 (2003).
[28] A. Kievsky *et al.* (in preparation, 2009).
[29] E. Huttel *et al.*, Nucl. Phys. **A406**, 435 (1983).
[30] C. R. Brune *et al.*, Phys. Rev. C **63**, 044013 (2001).
[31] A. Kievsky *et al.*, Phys. Rev. C **63**, 024005 (2001).
[32] D. C. Kocher and T. B. Clegg, Nucl. Phys. **A132**, 455 (1969).
[33] S. Shimizu *et al.*, Phys. Rev. C **52**, 1193 (1995).
[34] R. Sherr *et al.*, Phys. Rev. **72**, 662 (1947).
[35] M. H. Wood *et al.*, Phys. Rev. C **65**, 034002 (2002).
[36] H. Witala, D. Hüber, and W. Glöckle, Phys. Rev. C **49**, R14 (1994).
[37] A. Kievsky, M. Viviani, and S. Rosati, Phys. Rev. C **64**, 024002 (2001).
[38] R. K. Adair *et al.*, Phys. Rev. **89**, 1165 (1953).
[39] J. Weber *et al.*, Helv. Phys. Acta **54**, 547 (1981).
[40] E. M. Neidel *et al.*, Phys. Lett. **B552**, 29 (2003).
[41] P. Schwarz *et al.*, Nucl. Phys. **A398**, 1 (1983).
[42] J. E. McAninch, L. O. Lamm, and W. Haeberli, Phys. Rev. C **50**, 589 (1994).